Letter of Intent for a Super η/η'-Factory at GSI

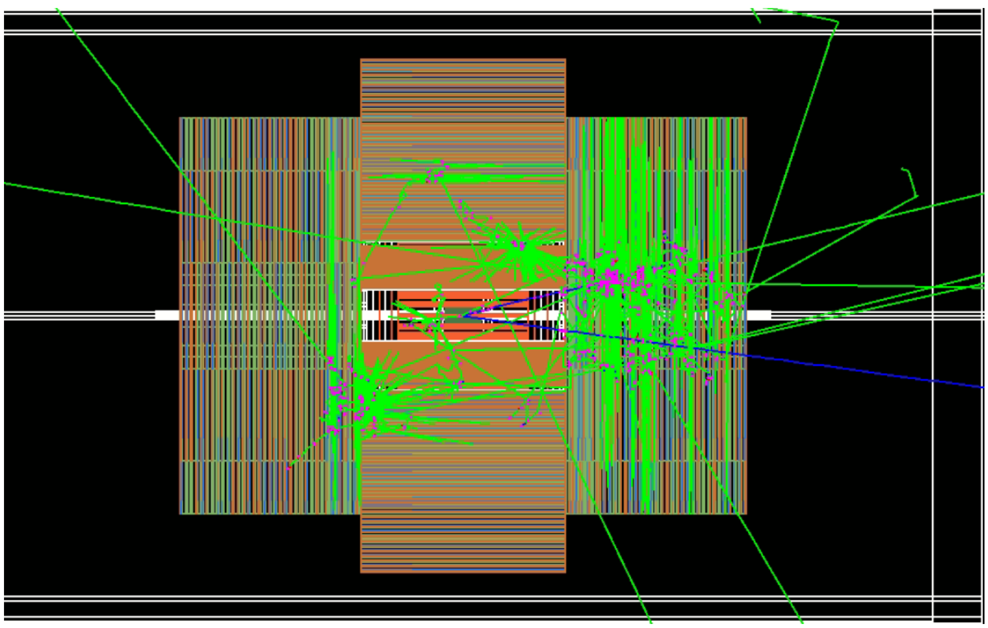

The REDTOP Experiment: Probing for New Physics with Rare η/η' Decays.

J. Elam, M. Jadhav, A. Mane, J. Metcalfe,[1] J. Comfort, P. Mauskopf, D. McFarland, L. Thomas,[2] I. Pedraza, D. Leon, S. Escobar, D. Herrera, D. Silverio,[3] B. Bilki,[4,5] W. Abdallah,[6] Z. Sheemanto,[7] D. Winn,[8] M. Spannowsky,[9] V. Di Benedetto, C. Johnstone, A. Kronfeld, E. Ramberg,[10] A. Alqahtani,[11] J. Shi,[12,13] R. Gandhi,[14] S. Homiller,[15] X. Chen, Q. Hu,[16] E. Passemar,[17,18] P. Sánchez-Puertas,[19] S. Roy,[20] C. Gatto,[21,22,*] W. Baldini,[23] R. Carosi, A. Kievsky, M. Viviani,[24] W. Krzemień, M. Silarski, M. Zielinski,[25] D. Guadagnoli,[26] D. S. M. Alves, S. González-Solís, S. Pastore,[27] V. Santoro,[28] M. Berlowski,[29] G. Blazey, A. Dychkant, K. Francis, M. Syphers, V. Zutshi, P. Chintalapati, T. Malla, M. Figora, T. Fletcher,[22] V. Pronskikh,[30] A. Ismail,[31] D. Egaña-Ugrinovic,[32] Y. Kahn,[33] J. Friese,[34] D. McKeen,[35] P. Meade,[36] A. Gutierrez-Rodriguez, M. A. Hernandez-Ruiz,[37] R. Escribano, P. Masjuan, E. Royo,[38,19] B. Kubis,[39] J. Jaeckel,[40] L. E. Marcucci,[41] C. Siligardi, S. Barbi, C. Mugoni,[42] M. Guida,[43] S. Charlebois, J. F. Pratte,[44] L. Harland-Lang,[45] Y. D. Tsai,[46]

R. Gardner, P. Paschos,[47] J. Konisberg,[48] C. Mills, Z. Ye,[49] M. Murray, C. Rogan, C. Royon, N. Minafra, A. Novikov, F. Gautier, T. Isidori,[49] C. Mills, Z. Ye,[49] S. Gardner, X. Yan,[50] Y. Onel,[5] M. Pospelov,[51] B. Batell, A. Freitas, M. Rai,[52] D. N. Gao,[53] K. Maamari,[54] A. Kupść,[55] B. Fabela-Enriquez,[56] A. Petrov,[57] and S. Tulin[58]
(REDTOP Collaboration)[†]

[1] *Argonne National Laboratory, (USA)*

[2] *Arizona State University, (USA)*

[3] *Benemerita Universidad Autonoma de Puebla, (Mexico)*

[4] *Beykent University, (Turkey)*

[5] *University of Iowa, (USA)*

[6] *Department of Mathematics, Faculty of Science, Cairo University, Giza (Egypt)*

[7] *City University of New York, (USA)*

[8] *Fairfield University, (USA)*

[9] *Durham University, (UK)*

[10] *Fermi National Accelerator Laboratory, (USA)*

[11] *Georgetown University, (USA)*

[12] *Guangdong Provincial Key Laboratory of Nuclear Science, Institute of Quantum Matter, South China Normal University, Guangzhou 510006, (China)*

[13] *Guangdong-Hong Kong Joint Laboratory of Quantum Matter, Southern Nuclear Science Computing Center, South China Normal University, Guangzhou 510006, (China)*

[14] *Harish-Chandra Research Institute, HBNI, Jhunsi (India)*

[15] *Harvard University, Cambridge, MA (USA)*

[16] *Institute of Modern Physics, Chinese Academy of Sciences, Lanzhou (China)*

[17] *Indiana University (USA)*

[18] *Institut de Física Corpuscular, Paterna (Spain)*

[19] *Institut de Física d'Altes Energies - Barcelona (Spain)*

[20] *Institute of Physics, Sachivalaya Marg, Sainik School Post, Bhubaneswar, (India)*

[21] *Istituto Nazionale di Fisica Nucleare – Sezione di Napoli, (Italy)*

[22] *Northern Illinois University, (USA)*

[23] *Istituto Nazionale di Fisica Nucleare – Sezione di Ferrara, (Italy)*

[24] *Istituto Nazionale di Fisica Nucleare – Sezione di Pisa, (Italy)*

[25] *Institute of Physics, Jagiellonian University, 30-348 Krakow, (Poland)*

[26] *Laboratoire d'Annecy-le-Vieux de Physique Théorique, (France)*
[27] *Los Alamos National Laboratory, (USA)*
[28] *Lund University, (Sweden)*
[29] *National Centre for Nuclear Research – Warsaw, (Poland)*
[30] *Oak Ridge national Laboratory, (USA)*
[31] *Oklahoma State University, (USA)*
[32] *Perimeter Institute for Theoretical Physics, Waterloo, (Canada)*
[33] *Princeton University, Princeton, (USA)*
[34] *Technical University of Munich, (Germany)*
[35] *TRIUMF, (Canada)*
[36] *Stony Brook University – New York, (USA)*
[37] *Universidad Autonoma de Zacatecas, (Mexico)*
[38] *Universitat Autónoma de Barcelona*
[39] *Universität Bonn, Helmholtz-Institut für Strahlen- und Kernphysik (Theorie) and Bethe Center for Theoretical Physics (Germany)*
[40] *Universität Heidelberg, (Germany)*
[41] *Universita' di Pisa and INFN, (Italy)*
[42] *Universita' di Modena e Reggio Emilia, (Italy)*
[43] *Universita' di Salerno and INFN – Sezione di Napoli, (Italy)*
[44] *Université de Sherbrooke, (Canada)*
[45] *University of Oxford, (UK)*
[46] *University of California Irvine, (USA)*
[47] *University of Chicago, (USA)*
[48] *University of Florida, (USA)*
[49] *University of Illinois Chicago, (USA)*
[50] *University of Kentucky, (USA)*
[51] *University of Minnesota, (USA)*
[52] *University of Pittsburgh, (USA)*
[53] *University of Science and Technology of China, (China)*
[54] *University of Southern California, (USA)*
[55] *University of Uppsala, (Sweden)*
[56] *Vanderbilt University, (USA)*

[57] *Wayne State University, (USA)*
[58] *York University, (Canada)*

(Dated: September 18, 2023)

* Email cgatto@na.infn.it[Corresponding author]
† Homepage: https://redtop.fnal.gov

CONTENTS

EXECUTIVE SUMMARY

Laboratories with high intensity proton accelerators have a unique opportunity to uncover dark matter or New Physics within a decade through production and study of extremely large η/η' samples.

An η/η' factory is an excellent laboratory for studying rare processes and Beyond Standard Model physics at low energy. There are strong theoretical reasons to search for New Physics in the MeV–GeV range. The η and η' mesons are unique particles since they carry the same quantum numbers as the Higgs (except for parity), and have no Standard Model charges. Their decays are flavor-conserving and most of them forbidden at leading order (in various symmetry-breaking parameters) within the Standard Model. New Physics must, also, be neutral under Standard Model charges: its production from the decay of the η and η' mesons would occur without Standard Model charged currents, opposite to the case of heavy flavor mesons. Rare decays are therefore enhanced compared to the remaining flavor-neutral mesons.

A sample of order $10^{14}(10^{12}\ )$ η/η' mesons can address most of the recent theoretical models. Such an experiment would have enough sensitivity to explore a very large portion of the unexplored parameter space for all the four portals connecting the Dark Sector with the Standard Model. Lepton Universality and the CP and T symmetries can also be probed with excellent sensitivity. Many other studies can be conducted with such a large data sample, including, for example, the determination of the η form factors, which is crucial to understanding the $(g-2)_\mu$ measurement.

The REDTOP Collaboration (comprised of 55 institutions) is proposing an η/η' factory. No similar experiment exists or is currently planned by the international scientific community. The accelerator complex available presently at GSI and the experimental infrastructure fulfill all requirements to achieve the proposed research program. Furthermore, the capabilities will be boosted once the new accelerator facility FAIR is taken into operation.

A detailed detector simulation and reconstruction has been implemented to study several processes driven by New Physics, and many theoretical models have been benchmarked. About 5×10^{10} background events have been generated and fully reconstructed to estimate the sensitivity of REDTOP. This took over three years to complete and required about 4×10^{7} core-hours of computing on the Open Science Grid.

The Physics case for REDTOP is presented in the first part of this document, along with the estimated sensitivity to the four portals and to the latest theoretical models proposed to explain outstanding experimental anomalies. We also discuss several tests of conservation laws which could be explored at REDTOP. The description of the REDTOP experiment, along with the estimated timeline and cost, is presented in the second part of this document.

I. INTRODUCTION

The Standard Model (SM) does not offer a complete description of all quantum interactions. The exact nature of dark energy and dark matter, the baryon asymmetry of the universe, the observed accelerating expansion of the Universe, and neutrino masses are among the very interesting questions that cannot be answered within the framework of the Standard Model (SM). There is a strong indication that the physics Beyond the Standard Model (BSM) could contain new particles and/or force mediators, which significantly violate some discrete symmetries of the universe, in particular *CP*.

The High Energy Physics (HEP) community has engaged in an unprecedented experimental effort, with the construction of the LHC and its four detectors, to observe BSM physics in the high energy domain. The absence of conclusive evidence so far may suggest that: a) New Physics (NP) most immediately accessible to experimenters is at *low* energies, rather than at high energies, and b) such NP is elusive, in particular it couples to SM matter too faintly to be detected by experiments at colliders. To detect such interactions, one may need larger luminosities, which are one of the most attractive features of fixed-target experiments. For the kind of NP mentioned above, low-energy fixed-target experiments with hadronic beams thus have well-defined advantages with respect to high-energy colliders as well as high-energy fixed-target experiment, where the background would overwhelm any signal produced at low energy.

Two of the most limiting factors in designing a high-intensity fixed target experiment are: a) the sheer production rate of events from inelastic interaction of the beam with the target and, b) the large background from neutrons (either primary or secondary) which make a signal in the detector. Regarding point a), the technologies implemented in the present generation of detectors are not fast enough to cope with proton beam intensities even as modest as a few tens of watts. Regarding point b), a neutron and a photon have very similar signatures in a conventional, single-readout calorimeter, hindering the ability to disentangle such particles unless novel detector techniques are implemented. Last, but not least, intense neutron fluxes could quickly damage a detector composed of non-radiation-hard materials. The design of the REDTOP experiment addresses these considerations.

REDTOP is a high yield η/η'-factory, operated in a fixed target configuration with beam luminosity of order 10^{34} cm^{-2}sec^{-1}. The mass range for potential discoveries is approximately [14 MeV-950 MeV], limited on the lower side by the resolution of the detector and on the upper side by the meson mass. REDTOP is also a frontier experiment, aiming at measuring the η/η' decay rates or their asymmetries for very rare processes, and with precision several orders of magnitude higher than present measurements. These decays would provide direct tests of conservation laws and, along with other measurements, will open up new windows to discover BSM physics.

To search for NP, REDTOP will involve the development and first use of innovative detectors. Novel instrumentation will include a super-light vertex detector, a Low Gain Avalanche Detector(LGAD)-based central tracker with unprecedentedly low material budget [1], a triple-readout calorimeter (ADRIANO3), and a Čerenkov Threshold Time-of-Flight

($CTOF$). An optional Active Muon Polarimeter is being considered to improve the measurements of the muon polarization.

II. MOTIVATIONS FOR A HIGH LUMINOSITY η/η' FACTORY

As has been noted elsewhere, "Light dark matter (LDM) must be neutral under SM charges, otherwise, it would have been discovered at previous colliders" [2]. Under such circumstances, the study of processes originated by particles carrying no SM charges is, intuitively, more appropriate in LDM searches, as no charged currents are present, which could potentially interfere with BSM processes.

The η and η' mesons have been widely studied in the past, as their special nature has attracted curiosity [3]. The η is a Goldstone boson, which strongly contraints its QCD dynamics. In nature, there are only few Goldstone bosons. Furthermore, the η is, at the same time, an eigenstate of the ***C, P, CP, I*** and ***G*** operators with all zero eigenvalues (namely: $I^G J^{PC} = 0^+0^{-+}$), identical (except for parity) to the vacuum or the Higgs boson. In that respect, it is a very pure state, carrying no SM charges and, as noted above, its decays do not involve charge-changing currents: all decays of η and η' mesons are flavor-conserving. Therefore, in some respects a η/η'-factory could be interpreted as a "low-energy Higgs-factory", anticipating much of the exploration achievable at a high-energy Higgs factory. Any coupling to BSM states, therefore, does not interfere with SM charge-changing operators (as occurs, for example, with mesons carrying flavor). From the experimental point of view, η/η' dynamics are particularly favorable to the exploration of small BSM effects since, as a consequence of the properties mentioned above, they have an unusually small decay width (Γ_η=1.3 KeV vs Γ_ρ=149 MeV, for example). Electromagnetic and strong decays are suppressed up to order $\mathcal{O}(10^{-6})$, favoring the study of more rare decays, especially those related to BSM particles and to violation of discrete symmetries. This helps considerably in reconstructing the kinematics of the events and in reducing SM background by requiring consistency of the invariant mass of the final state particles with the η mass.

Another reason to precisely investigate the η/η' mesons is that their structure has never been fully understood. Recent work [4] indicates that such mesons are unique among the pseudoscalars as they have anomalously large masses for which quarks contribute only about 80% of the momentum, leaving considerable room for potential contributions by NP. A summary of the processes that can be studied at REDTOP for exploring NP is shown in Fig. 1. The processes are grouped by their physics topic, and some will be discussed in more detail in the next sections.

Considering the present limits on the parameters associated with BSM physics and the practical limitations of current detector technologies, the next generation of experiments should be designed with the goal of producing no less than 10^{13} η mesons and 10^{11} η' mesons. The physics reach of an experiment with such statistics is very broad, spanning several aspects of BSM physics. The most relevant processes to be explored fall into two main fields of research: *Searches for New Particles and Fields*, and *Tests of Conservation Laws.* Along with BSM physics, the availability of such a large sample of flavor-conserving mesons

C, T, CP-violation

- CP Violation via Dalitz plot mirror asymmetry: $\eta \to \pi^0\pi^+\pi^-$
- CP Violation (Type I - P and T odd , C even): $\eta \to 4\pi^0 \to 8\gamma$
- CP Violation (Type II - C and T odd , P even): $\eta \to 4\pi^0 l^+ l^-$ and $\eta \to 3\gamma$
- CP invariance via μ longitudinal polarization: $\eta \to \mu^+\mu^-$
- CP invariance via γ^* polarization studies: $\eta \to \pi^+\pi^- e^+ e^-$ and $\eta \to \pi^+\pi^-\mu^+\mu^-$
- CP invariance in angular correlation studies: $\eta \to \mu^+\mu^- e^+ e^-$
- CP invariance in μ polarization studies: $\eta \to \mu^+\mu^-$
- T invariance via μ transverse polarization: $\eta \to \pi^0\mu^+\mu^-$ and $\eta \to \gamma\mu^+\mu^-$
- CPT violation: μ polarization in $\eta \to \pi^+\mu^-\nu$ vs $\eta \to \pi^-\mu^+\nu$ and γ polarization in $\eta \to \gamma\gamma$

New particles and forces searches

- Scalar meson searches (charged channel): $\eta \to \pi^0 H$ with $H \to e^+e^-$ and $H \to \mu^+\mu^-$
- Dark photon searches: $\eta \to \gamma A'$ with $A' \to l^+ l^-$
- Protophobic fifth force searches: $\eta \to \gamma X_{17}$ with $X_{17} \to e^+e^-$
- QDC axion searches: $\eta \to \pi\pi a_{17}$ with $a_{17} \to e^+e^-$
- New leptophobic baryonic force searches: $\eta \to \gamma B$ with $B \to \pi^+ pi^-$ or $B \to \gamma\pi^0$
- Indirect searches for dark photons new gauge bosons and leptoquark: $\eta \to \mu^+\mu^-$ and $\eta \to e^+e^-$
- Search for true muonium: $\eta \to \gamma(\mu^+\mu^-)|_{2M_\mu} \to \gamma\, e^+e^-$
- Lepton Universality
- $\eta \to \pi^0 H$ with $H \to \nu N_2$, $N_2 \to h' N_1$, $h' \to e^+e^-$

Other discrete symmetry violations

- Lepton Flavor Violation: $\eta \to \mu^+ e^- + c.c.$
- Radiative Lepton Flavor Violation: $\eta \to \gamma\mu^+ e^- + c.c.$
- Double lepton Flavor Violation: $\eta \to \mu^+\mu^+ e^- e^- + c.c.$
- Lepton Number Violation: $\eta \to \pi^-\pi^- e/\mu^+ e/\mu^+ c.c.$

Other Precision Physics measurements

- Proton radius anomaly: $\eta \to \gamma\,\mu^+\mu^-$ vs $\eta \to \gamma\, e^+e^-$
- All unseen leptonic decay mode of η/η'(SM predicts $10^{-6} \div 10^{-9}$)

Non-η/η' based BSM Physics

- Dark photon and ALP searches in Drell-Yan processes: $q\bar{q} \to A'/a \to l^+ l^-$
- ALP's searches in Primakoff processes: $pZ \to pZa \to l^+ l^-$ (F. Kahlhoefer)
- Charged pion and kaon decays: $\pi^+ \to \mu^+\nu A' \to \mu^+\nu e^+ e^-$ and $K^+ \to \mu^+\nu A' \to \mu^+\nu\, e^+e^-$
- Neutral pion decay: $\pi^0 \to \gamma A' \to \gamma\, e^+e^-$

High precision studies on medium energy physics

- Nuclear models
- Chiral perturbation theory
- Non-perturbative QCD
- Isospin breaking due to the u-d quark mass difference
- Octet-singlet mixing angle
- Electromagnetic transition form-factors (important input for g-2)

FIG. 1. Physics landscape for a η/η' factory.

will also allow probing the isospin violating sector of low energy QCD to an unprecedented degree of precision.

The large number of processes that could be studied at the proposed η/η'-factory will provide not only a nice scientific laboratory but also the source of many topics for Ph.D. thesis. Fig. 1 suggests forty or more channels are available for thesis opportunities. A few of the BSM processes accessible with an η/η'-factory of REDTOP class have been selected for detailed sensitivity studies. They will be discussed later in this paper, along with several recent theoretical models which explain anomalies that have been observed by the experiments.

III. BSM PHYSICS WITH REDTOP

Large samples of η/η' decays open new avenues for the study of BSM physics. This is particularly true for weakly coupled hidden sectors, in which the new fields are Standard Model singlets, as well as studies of fundamental symmetries and their breaking. REDTOP is capable of probing all of these portals. Turning to symmetry tests, REDTOP offers new opportunities for searches for CP violation, as well as for tests of both lepton flavor violation and universality. Within the standard model CP violation is described by one complex phase in the Cabibbo-Kobayashi-Maskawa (CKM) quark-mixing matrix. It has long been suspected new sources of CP violation must exist in order to explain baryon asymmetry of the universe. Tantalizing hints of lepton-flavor-universality violation have also been seen in B-meson decays, and it is important to search for these effects in light-quark systems as well. Searches for lepton-flavor violation in η, η' decays complement searches for $\mu - e$ conversion in the field of a nucleus, for which sensitive searches are being mounted worldwide.

Figure 1 provides a compact illustration of the physics possibilities. The overview that follows describes these possibilities, noting the golden channels that have a higher signal to background ratio within REDTOP.

Physics studies were performed to estimate the sensitivity of REDTOP to several benchmark BSM processes and several theoretical models. The studies are based on the Snowmass-2021 detector layout and advanced simulations, described in detail in the REDTOP white paper [5]. The sensitivity curves correspond to an integrated proton yield of 3.3×10^{18} POT. According to the analysis performed in Sec. V B, that is achievable with an effective running time of 12 months. Here, we present selected results.

A. Searches for new particles and fields

One of the most prominent ways to accommodate new particles is hidden sector physics, comprising new particles with masses below the electroweak scale coupled very weakly to the Standard Model world via portals [6]. Such schemes are characterized by new particles which are either heavy or interact indirectly with the Standard Model sector. These hidden sectors may be experimentally accessible via particles in the MeV–GeV mass range, which are coupled to the Standard Model sectors via renormalizable interactions with dimensionless coupling constants (the portals) or by higher-dimensional operators. Several η/η' related processes have been selected to study the sensitivity of REDTOP to such portals. Some of them could also shed light on anomalies observed in recent experiments. These searches are golden opportunities for REDTOP.

1. Vector portal

Several extensions of the standard model are based on the interaction of new light vector particles, resulting, for example, from extra gauge symmetries. New vector states can mediate interactions both with the Standard Model fields, and with extra fields in the dark sector. It is speculated that the gauge structure of the Standard Model derives from a larger gauge group, as, for example, in the Grand Unified Theories (GUTs), where new vector states exist. If these particles exist, their mass is expected to be of the order of 10^{16} GeV, an energy well beyond the direct reach of present accelerators. Other models assume that the Standard Model has additional gauge structures able to accommodate gauge bosons with masses below the TeV scale [7]. Current results from LHC experiments have put very strong bounds on the existence of such new vector states, with the hypothesis that the coupling of the latter to the Standard Model is large enough. To cope with such observations, more recent theoretical models assume the existence of relatively light vector states (e.g., in the MeV–GeV mass range) with small couplings to the Standard Model. This mass range is poorly constrained by the LHC experiments, and it could be probed easily with dedicated experiments with high intensity beams such as η/η'-factories.

The vector portal can be probed via radiative decays of the η-meson and its subsequent decay into a lepton-antilepton $\ell\bar{\ell}$ pair or into two pions. The processes considered here are $p + Li \to \eta + X$ with $\eta \to \gamma A'$ and $A' \to e^+e^-$, $\to \mu^+\mu^-$, and $\to \pi^+\pi^-$. Two different analyses were performed, aiming at testing the performance of different components of the detector: a *bump-hunt* and a *detached-vertex* analysis.

The *bump-hunt* analysis assumes that the vector particle has a decay length not resolvable by the tracking system. In this case, the process is identified only from its kinematics, in particular by observing a bump in the invariant mass of the $\ell\bar{\ell}$ or the $\pi^+\pi^-$ system. The total reconstruction efficiency for this process was found to be between $\sim$9% and $\sim$22% for the signal samples and of order $\mathcal{O}(10^{-9})$ for the Urqmd background, with a strong dependence on the e^+e^- invariant mass.

The *detached-vertex* analysis aims at evaluating the sensitivity of the detector to events with a long-lived particle decaying into a lepton pair and a secondary vertex detached from the η production vertex. A similar event topology is not known to be caused by any Standard Model process. Thus, the rejection of the background with the *detached-vertex* analysis is expected to improve considerably compared to the *bump-hunt* analysis. The final reconstruction efficiency for this process, including the additional vertex cuts, was found to be between $\sim$2% and $\sim$10% for the signal samples and of order $\mathcal{O}(10^{-10})$ for the Urqmd background. The resulting branching ratio sensitivity is shown in Fig. 2, as a function of the invariant mass of the vector boson. The error bars are statistical only.

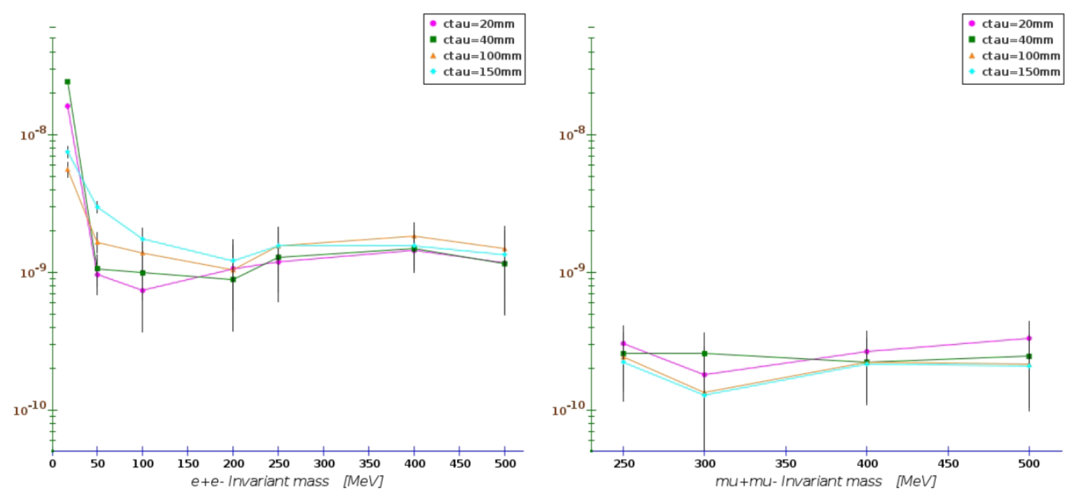

FIG. 2. Branching ratio sensitivity for the process $\eta \to \gamma A'$; $A' \to e^+e^-$ (left) and $\eta \to \gamma A'$; $A' \to \mu^+\mu^-$ (right) as a function of the mass and $c\tau$ of the a long-lived vector boson A'.

A similar analysis was conducted for the $A' \to \mu^+\mu^-$ and for $\eta \to \gamma B$; $B \to \pi^+\pi^-$ processes. The former also probes the lepton flavor dependence of the A' vector. The branching ratio sensitivity of the latter is somehow lower, due to the strong suppression of hadronic final states by the trigger of the experiment. The sensitivity curves are shown, respectively, in Fig. 2 and Fig. 3. A detailed discussion of the analyses can be found in reference [5].

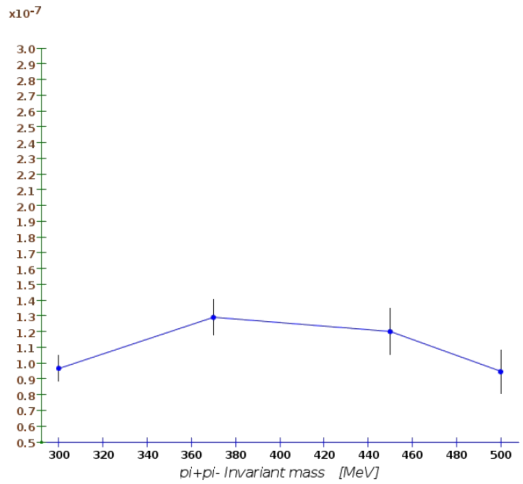

FIG. 3. Branching ratio sensitivity for the process $\eta \to \gamma B$; $B \to \pi^+\pi^-$ with the bump-hunt analysis

We benchmarked four distinct theoretical models, for which New Physics appears through the vector portal. More specifically, the branching ratio sensitivity obtained in the previous sections is used to determine the sensitivity to the corresponding coupling constants. Theoretical Models are the Minimal dark photon model, the Leptophobic B boson Model, the Protophobic Fifth Force.

For sake of conciseness, we report the results for one of the most popular models in the Vector portal is commonly referred to as Minimal dark photon model. In this case, the Standard Model is augmented by a single new state A' which couples to visible matter via a kinetic mixing parameter ε [8]. This model predicts a relatively large branching ratio for the processes: $\eta/\eta' \to \gamma A' \to \gamma e^+e^-$ and $\eta/\eta' \to \gamma A' \to \gamma\mu^+\mu^-$. REDTOP will be able to detect a number of such final states with samples larger than 10^8. The relevant parameter of this model is the kinetic mixing ϵ^2 We show the plot for the corresponding sensitivity of ε^2 in Fig. 4 for the *bump-hunt* and the *detached-vertex* analyses superimposed to the constraints from previous measurements. REDTOP will be able to probe most of the unexplored ε^2 parameter space.

The benchmarks for the Leptophobic B boson Model and the Protophobic Fifth Force models can be found in reference [5].

2. Scalar portal

In the scalar portal the dark sector couples to the Standard Model via the Higgs boson or an extension of the latter. Several theoretical models exists: three complementary models are currently under consideration by REDTOP, the *Minimal dark scalar model, Spontaneous Flavor Violation model* or *Flavor-Specific Scalar model* (which have similar

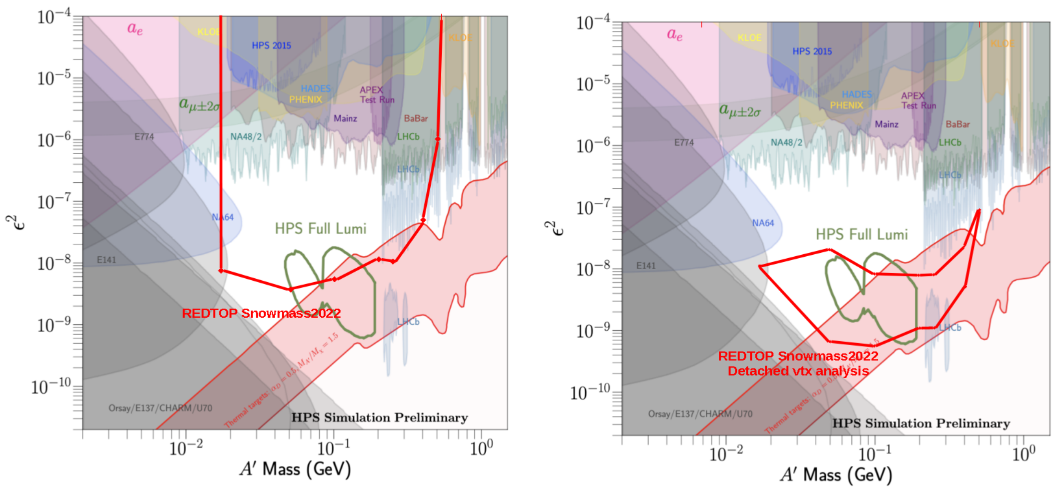

FIG. 4. Sensitivity to to ε^2 for the processes $\eta \to \gamma A'$ for integrated beam flux of 3.3×10^{18} POT. Left plot: bump-hunt analysis. Right plot: detached-vertex analysis).

REDTOP phenomenology), and the *Two-Higgs doublet model.* In the former, the dark scalar mimics a light Higgs and, consequently, it couples dominantly to heavy quarks. The latter has larger coupling, instead, to light quarks. The predicted branching ratios for the two models differ by more than two orders of magnitude. The *Scalar portal* can be probed via decays of the η-meson with a π^0 meson in association with either two leptons or two pions. As for the case of the *Vector portal*, a *bump-hunt* and a *detached-vertex* analysis were performed to test the performance of different components of the detector. The branching ratio sensitivities for these processes are shown in Fig. 5 for the *bump-hunt* case and in Fig. 6 for the *detached-vertex* analyses, as a function of the invariant mass of the scalar boson. A detailed discussion of the analyses can be found in reference [5]. *Webenchmarkedthreedistincttheoreticalmodels*,for which New Physics appears through the scalar portal: the *Minimal scalar model*, the *Spontaneous Flavor Violation model*, and the *Two-Higgs doublet model.*

The *minimal scalar portal* model operates with one extra singlet field S and two types of couplings, μ and λ. The mechanism for the $\eta \to \pi^0\mu^+\mu^-$ (or e^+e^-) decay is usually described via a 2-photon intermediate state to conserve C via a triangle diagram, $\eta \to \pi^0\gamma\gamma$ along with $\gamma\gamma \to \mu\bar{\mu}$. Branching ratios are calculated to be of the order of 10^{-9} [9–12], which should be well within the sensitivity of REDTOP. The relevant parameter in this case is the mixing angle θ^2 [13] between the Standard Model Higgs and its lighter counterpart. In the Tulin parametrization of the *Minimal Scalar model* the master formula for $Br(\vartheta^2)$ is [14]:

$$BR_{\eta \to \pi^0 h} \approx 1.8 \times 10^{-6} \times \lambda^{1/2}\left(1, \frac{M_{\pi_0}^2}{M_\eta^2}, \frac{M_H^2}{M_\eta^2}\right) \tag{1}$$

where the function λ has been defined in reference [5]. Inserting in Eq. (1) the values of the

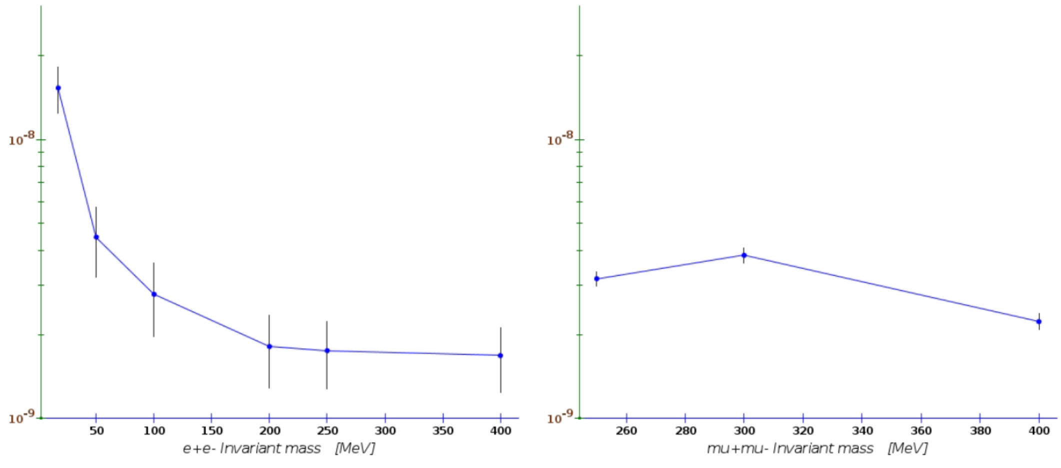

FIG. 5. Branching ratio sensitivity for *bump-hunt* analyses of the process $\eta \to \pi^0 h$; $h \to e^+e^-$ (left) and $\eta \to \pi^0 h$; $h \to \mu^+\mu^-$ (right) as a function of the mass of the scalar boson h.

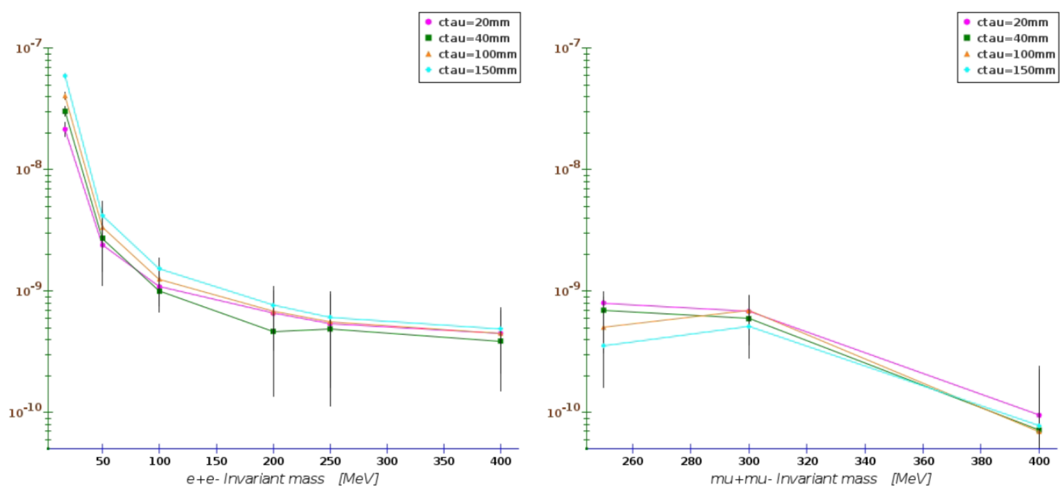

FIG. 6. Branching ratio sensitivity for *detached-vertex* analyses of the process $\eta \to \pi^0 h$ *and* $h \to e^+e^-$ (left) and $\eta \to \pi^0 h$; $h \to \mu^+\mu^-$ (right) as a function of the mass and $c\tau$ of a long-lived scalar boson h.

branching ratio sensitivity derived for each value of the h mass, we obtain the corresponding plots of sensitivity for the parameter θ^2. They are shown in Fig. 7 for the *bump-hunt* analyses of the two leptonic final states and in Fig. 8 for the two *detached-vertex* analyses. A second parametrization of Eq. (1) (*Pospelov parametrization*) is discussed in detail in reference [5].

It has been stressed in Ref. [15] that REDTOP has excellent prospects to probe scalars that couple dominantly to first generation quarks. In the *Spontaneous Flavor Violation models* the scalar S couples prevalently to up quarks. The *hadrophilic scalar mediator* is a particular implementation of the latter. The scalar will be produced via $\eta \to \pi^0 S$, with

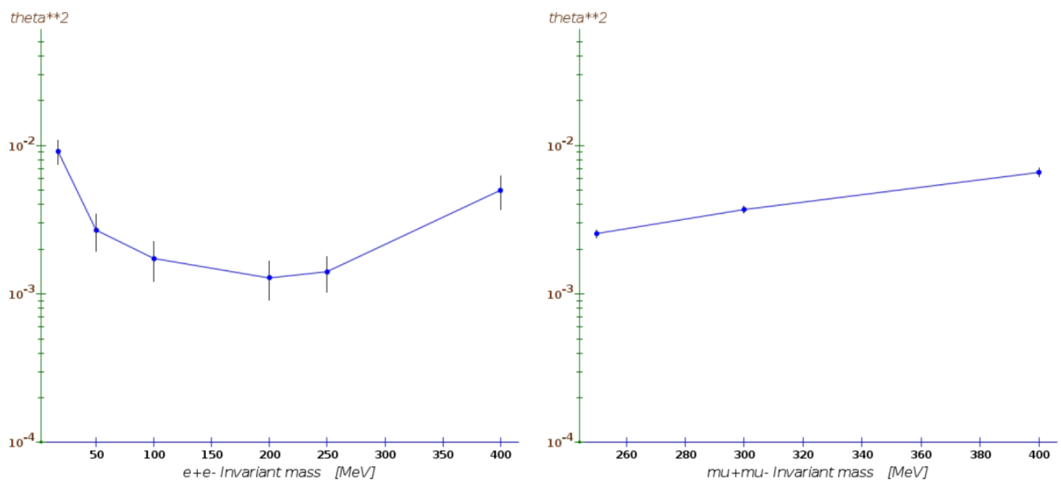

FIG. 7. Sensitivity to θ^2 in the Tulin approach[14] for the bump-hunt analysis of the processes $\eta \to \pi^0 h$ *and* $h \to e^+e^-$ (left) and $\eta \to \pi^0 h$ *and* $h \to \mu^+\mu^-$ (right) as a function of the mass of a short-lived scalar h.

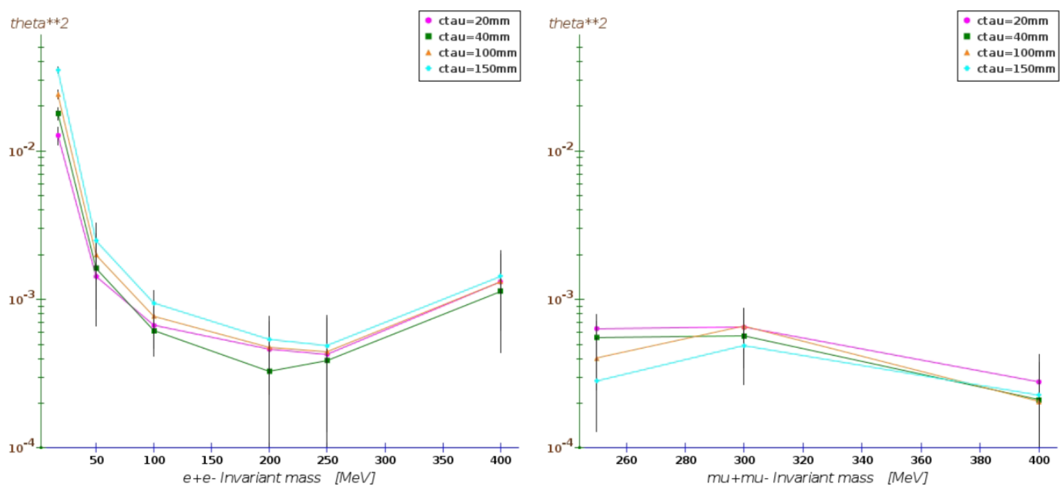

FIG. 8. Sensitivity to θ^2 for the bump-hunt analysis of the processes $\eta \to \pi^0 h$ *and* $h \to e^+e^-$ (left) and $\eta \to \pi^0 h$ *and* $h \to \mu^+\mu^-$ (right) as a function of the mass and $c\tau$ of the a long-lived scalar h.

branching ratio

$$\mathrm{Br}(\eta \to \pi^0 S) \;=\; \frac{c^2_{S\pi^0\eta} g_u^2 B^2}{16\pi m_\eta \Gamma_\eta} \lambda^{1/2}\left(1, \frac{m_S^2}{m_\eta^2}, \frac{m_{\pi^0}^2}{m_\eta^2}\right), \tag{2}$$

where $\lambda(a,b,c) = a^2 + b^2 + c^2 - 2ab - 2ac - 2bc$, $B \simeq m_\pi^2/(m_u + m_d) \approx 2.6$ GeV, and the coefficients $c_{S\pi^0\eta} = \frac{1}{\sqrt{3}}\cos\theta - \sqrt{\frac{2}{3}}\sin\theta$ parameterize the effects of $\eta - \eta'$ mixing, with $\theta \approx -20°$.

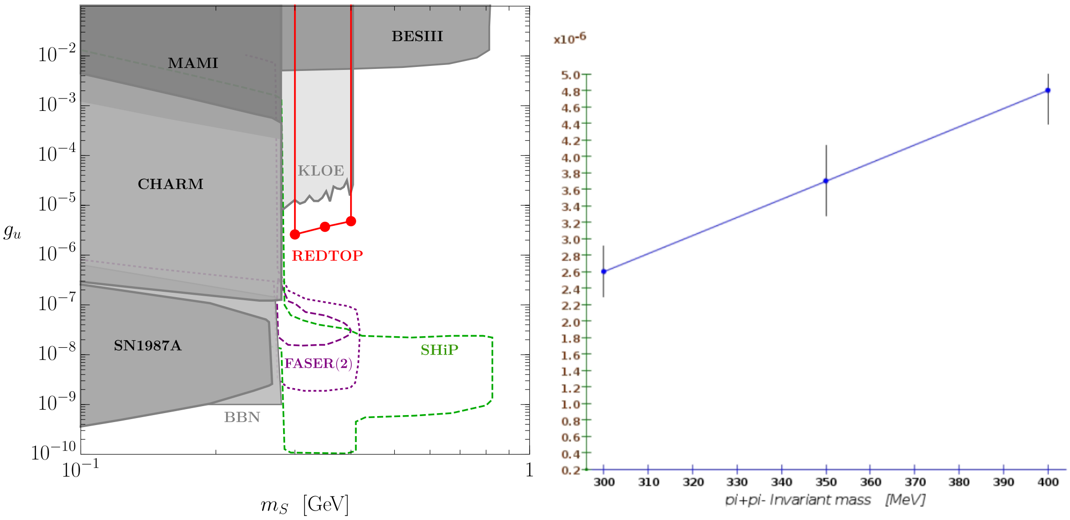

FIG. 9. REDTOP sensitivity to the the *hadrophilic scalar mediator*, Eq. (**??**), in the $\eta \to \pi^0 S$, $S \to \pi^+\pi^-$ mode. We display the projected sensitivity of REDTOP (red) in the $m_S - g_u$ plane a the bump hunt analysis (cfr. reference [5]) based on 3.3×10^{18} POT for the three mass points $m_S = 300, 350, 400$ MeV. Also shown are various existing constraints and projections from other planned or proposed experiments; see Refs. [15, 16] for further details.

m_{N_1}	m_{N_2}	m_{N_3}	$y_u^{h'(H)} \times 10^6$	$y_{e(\mu)}^{h'} \times 10^4$	$y_{e(\mu)}^{H} \times 10^4$
85 MeV	130 MeV	10 GeV	0.8(8)	0.23(1.6)	2.29(15.9)

$m_{h'}$	m_H	$\sin\delta$	$y_d^{h'(H)} \times 10^6$	$y_{\nu_{12}}^{h'(H)} \times 10^3$	$\lambda_{N_{12}}^{h'(H)} \times 10^3$
17 MeV	750 MeV	0.1	0.8(8)	1.25(12.4)	74.6(−7.5)

TABLE I. Benchmark point for LSND and MB events, and muon $g-2$ calculation.

The scalar decays promptly in the parameter region of interest to REDTOP. The sensitivity of REDTOP to the parametr g_u is shown in Figure. 9 (on the left, superimposed on the parameter space explored by previous experiments). The sensitivity curve indicates that REDTOP will probe couplings of order $g_u \sim \text{few} \times 10^{-6}$, extending the reach by a factor of a few beyond previous recasted bounds from the KLOE experiment [15, 17]. Furthermore, it is worth highlighting that REDTOP nicely complements the sensitivity from proposed long-lived particle searches at FASER [16], FASER2 [16] and SHiP [15], which will be able to explore longer lifetimes and smaller couplings.

The *Two-Higgs doublet model* model [18] is one of the simplest possible extensions of the Standard Model, assuming the existence of a second Higgs doublet H and a dark singlet real scalar h'. It was initially introduced to explain the anomalies observed by LSND, MiniBooNE and muon g−2 experiment, and it is being extended to the decays of the $\eta \to \pi^0 h'/H$ and $\eta' \to \pi^0 h'/H$. Preliminary calculations indicate that BR$(\eta \to \pi^0 h')\sim 10^{-9}$ while BR$(\eta' \to \pi^0 H)\sim 10^{-10}$, in both cases within REDTOP sensitivity.

The benchmark parameter values used for the sensitivity calculations are shown in Table I, where $\lambda_q^{h'(H)} = y_q^{h'(H)}$, $q = u, d$, and $\lambda_s^{h'(H)} = 0$, the partial decay widths. The branching ratio of $\eta \to \pi^0 S$ predicted by this model approximately equals to:

$$\mathrm{BR}(\eta \to \pi^0 S) \simeq \frac{2}{3} B_0^2 \frac{(\lambda_u - \lambda_d)^2}{\Gamma_\eta^{\mathrm{tot}}} \frac{\sqrt{\tilde{E}_\eta^2 - m_{\pi^0}^2}}{8\pi m_\eta^2}, \tag{3}$$

where

$$\tilde{E}_\eta = \frac{m_\eta^2 + m_{\pi^0}^2 - m_S^2}{2m_\eta}. \tag{4}$$

In this model [18], for non-zero difference of $(\lambda_u - \lambda_d)^2$, $\mathrm{BR}(\eta \to \pi^0 h')$ range is of order $\mathcal{O}(10^{-11} - 10^{-5})$ with $m_{h'} \simeq 17$ MeV. We can conclude that REDTOP is very sensitive to a mismatch in λ_u and λ_d values that keeps the LSND and MB fit intact. The corresponding sensitivity for the parameter $(\lambda_u - \lambda_d)^2$ is shown in Table II for the two analysis techniques we have used.

Process	m_S	*Analysis*	$(\lambda_u - \lambda_d)^2$ sensitivity
$\eta \to \pi^0 S$; $S \to e^+e^-$	17 MeV	bump hunt	2.0×10^{-13}
$\eta \to \pi^0 S$; $S \to \mu^+\mu^-$	17 MeV	detached vertex	3.2×10^{-13}

TABLE II. Sensitivity to $(\lambda_u - \lambda_d)^2$ for the process $\eta \to \pi^0 S$ and $S \to e^+e^-$ and $S \to \mu^+\mu^-$.

3. Pseudoscalar portal

The Pseudoscalar portal is a very rich sector of BSM physics and several novel theoretical models are predicting the existence of a new pseudoscalar state. Among others, the long-sought [19], but never confirmed, Peccei-Quinn model introduces an axion particle which could explain several anomalies recently observed by experiments. The Pseudoscalar portal can be probed at REDTOP via decays of the η-meson associated to two charged or neutral pions. In this work, we have considered leptonic, radiative, and hadronic decays of the pseudoscalar boson a.

The original incarnation of the QCD axion (the so-called 'PQWW' axion [19–22]) was a simple Two-Higgs-Doublet Model (2HDM) with a common breaking mechanism for the Electroweak and PQ symmetries. By the late 80s, the parameter space of the PQWW axion was fully excluded by searches for axionic production in hadronic decays and beam dump experiments. Still, many variants of the original QCD axion have been explored (see, e.g., [23]), and more recently, Alves and Weiner have shown that a variant of the QCD axion with $m_a \sim \mathcal{O}(1 - 10)$ MeV and $f_a \sim \mathcal{O}(1 - 10)$ GeV remains viable [24]. More generally, axio-hadronic decays of the η and η' can also probe axion-like particles (ALPs), which have the same types of interactions as the QCD axion but receive an additional, PQ-breaking contribution to their masses.

Another important class of models falling into this sector is are those which have Axion-Like Particles (ALP's). These models have extensions of the axion particle with relaxed constraints. As such, ALP models have a broader parameter space than the QCD axion since the ALP mass and decay constant are independent parameters. The processes studied are:

- $p + Li \to \eta + X$ with $\eta \to \pi^+\pi^- a$ and $a \to e^+e^-$
- $p + Li \to \eta + X$ with $\eta \to \pi^0\pi^0 a$ and $a \to e^+e^-$
- $p + Li \to \eta + X$ with $\eta \to \pi^+\pi^- a$ and $a \to \gamma\gamma$

Again, two different analysis were performed, aiming at testing the performance of different components of the detector: a *bump-hunt* and a *detached-vertex* analysis. The resulting

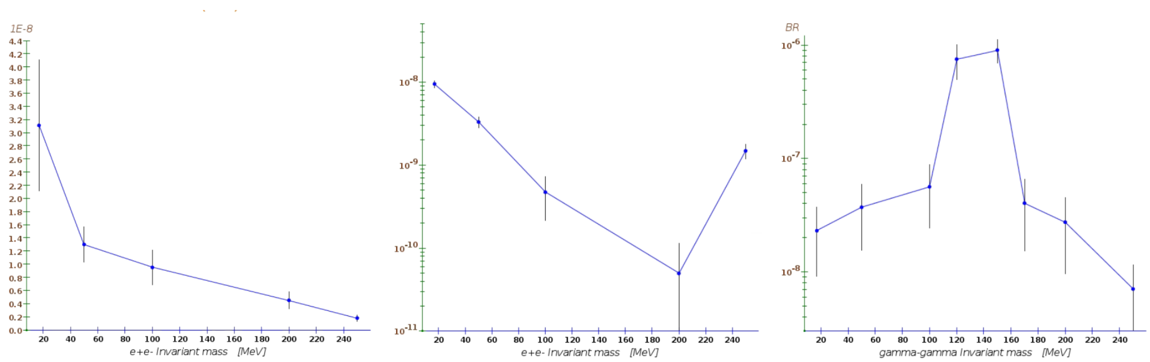

FIG. 10. Branching ratio sensitivity for the process $\eta \to \pi^0\pi^0 a$ with $a \to e^+e^-$ (right), $\eta \to \pi^+\pi^- a$ with $a \to e^+e^-$ (center), and $\eta \to \pi^+\pi^- a$ with $a \to \gamma\gamma$ 9left) as a function of the pseudoscalar boson mass M(a).

sensitivities are shown in Fig. 10 as a function of the pseudoscalar boson a mass. As expected, the process has a lower sensitivity for values of M(a) below 50 MeV, due to the large contribution of the $\gamma \to e^+e^-$ background. On the other side, the sensitivity is of order $\mathcal{O}(10^{-9})$ for higher mass values. The study of the $a \to \gamma\gamma$ decay is restricted, in the present work, to the bump-hunt analysis only, since the reconstruction of a detached $\gamma\gamma$ vertex is beyond the current capabilities of the reconstruction software. Two models, related to the pseudoscalar portal, have been considered for REDTOP studies: the *piophobic axion model*, the *axion-like particles* with eitherquark dominance, or with gluon dominance.

The *piophobic axion model* is particularly interesting since it pushes the limits on the mass of the QCD axion within the sensitivity of REDTOP. In order to estimate the sensitivity of the experiment to this model, the distribution of the axion momentum for M(a)=17 MeV, is fitted using the the theoretical matrix element from [25], combined with a second degree polynomial describing the background. The analysis was repeated for three sets of parameters of the model. The χ^2 probability to the fit each set of the parameters $+$is summarized in Table III.

POT	$\eta \rightarrow \pi^+\pi^- a$; $a \rightarrow e^+e^-$ Benchmark set	BR statistical error	χ^2/ndof
1.1×10^{13}	B1	1.5%	3.2
1.3×10^{13}	B2	1.4%	2.9
5.6×10^{12}	B3	2.1%	3.5

TABLE III. Goodness of fit of the P_{axion} distribution using the matrix element from Ref. [25]

A statistical error of $< 2\%$ indicates an excellent sensitivity of REDTOP to the *piophobic axion model* model.

The ALP's have the same types of interactions as the QCD axion but receive an additional, PQ-breaking contribution to their masses. As such, ALP models have a broader parameter space than the QCD axion since the ALP mass and decay constant are independent parameters. The formalism for the discussion of this class of models is presented in Sec. III.A.5 of Ref. [5]. The relevant parameters in this model are the coupling constants c_{GG}, c_q and the ALP decay constant f_a defined in Eq. 32 of [5]. For the determination of REDTOP sensitivity to c_{GG} and c_q, we made the conservative assumption that the a decays only into Standard Model particles. In that case, the values of the coupling constants are also related to the width of a, and, consequently, to the capability of the detector to reconstruct detached vertices.

Using the branching ratios values shown in Fig. 10, the corresponding sensitivity curves for c_{GG}/f_a and $c_q/f_a(= c_{QQ}/f_a)$ are shown in Fig, 11, for the final states considered in this work.

4. Heavy neutral lepton portal

This portal operates with one or several dark heavy neutral leptons (HNLs). Among the several models existing under this portal, the Two-Higgs doublet model is the only one considered, at present, by REDTOP. The process considered is: $\eta/\eta' \rightarrow \pi^0 H$ with $H \rightarrow \nu N_2$ and $N_2 \rightarrow h' N_1$ followed by $h' \rightarrow e^+e^-$. The process is identified by the presence of a π^0 and an e^+e^- pair in the final state and a peak in the missing mass of the η/η' spectrum. The reconstruction efficiencies for this process and for the Urqmd generated background are summarized in Table IV.

The parameters λ_u and λ_d for this model, along with the branching ratios predicted for decay channels $\eta^{(\prime)} \rightarrow \pi^0 S$ are discussed in Sec. III A 2. For the Two-Higgs doublet model considered in this work [18], the branching ratio, in the assumption that $\lambda_u = \lambda_d$, is predicted to be of order $\mathcal{O}(10^{-13})$, which is below REDTOP sensitivity in the present run. The situation is different when $\lambda_u \neq \lambda_d$. In that case, assuming the values for the branching ratios of the H defined in Eqs. (114),(115) and the branching ratios of the N_2 and h' defined

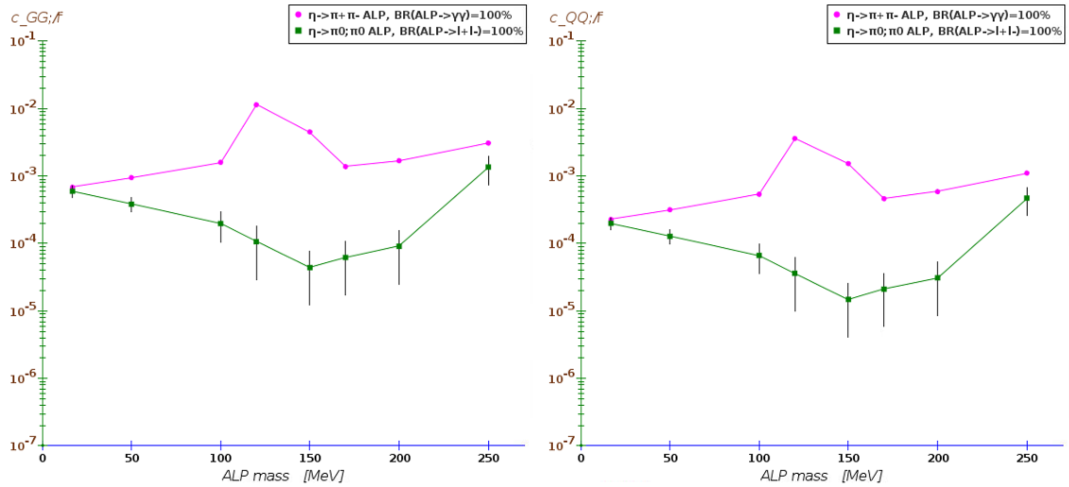

FIG. 11. Sensitivity to c_{GG}/f_a (left) and $c_{QQ}/f_a(= c_q/f_a)$ (right) for the processes $\eta \to \pi^+\pi^- a$ and $\eta \to \pi^o\pi^o a$ as a function of the mass of a the ALP a. The magenta curves refer to the decay $a \to e^+e^-$ while the green curves are for the case: $a \to \gamma\gamma$. See text for details of the analysis.

Process	*Trigger* L0	*Trigger* L1	*Trigger* L2	*Reco*	*Analysis*	**Total**	**BR Sensitivity**
$\eta \to \pi^0 H$; $H \to \nu N_2$; $N_2 \to N_1 h'$; $h' \to e^+e^-$	38.5%	22.6%	80.5%	91.1%	19.6%	1.3%	$2.7 \times 10^{-7} \pm 7 \times 10^{-9}$
Urqmd	21.7%	1.7%	22.2%	47.7%	0.17%	6.6×10^{-5}%	

TABLE IV. Reconstruction efficiencies and branching ratio sensitivity for $\eta \to \pi^0 H$; $H \to \nu N_2$; $N_2 \to N_1 h'$; $h' \to e^+e^-$ and for the Urqmd generated background with the parameters used in Table IV.

in Eqs. (29),(30) of Ref. [5], we derive a sensitivity to $(\lambda_u - \lambda_d)^2$ of 3.89×10^{-12}. The final value is shown in Fig. 12 superimposed to the prediction of the theoretical model.

B. Tests of conservation laws

Conservation laws with their underlying symmetry principles are at the heart of physics, from the classical space-time conservation laws of introductory courses through the symmetries and additive quantum numbers of modern particle physics. Recently, WASA at COSY reached a milestone, by collecting about 10^9 (in $pp \to pp\eta$), where the data has not yet been fully analyzed and the employed conventional detector technologies are likely insufficient for successfully exploring the realm of BSM. To reach the more exacting levels needed for symmetry violations, the usable η flux must be increased by several orders of magnitude. The light pseudoscalar mesons π^0, η, and η' have very special roles for exploring and testing the conservation laws. The π^0 has a long history of such tests and has established tight upper limits of charge (C) and lepton flavor (LF) violations [26]. Unlike the isospin $I = 1$

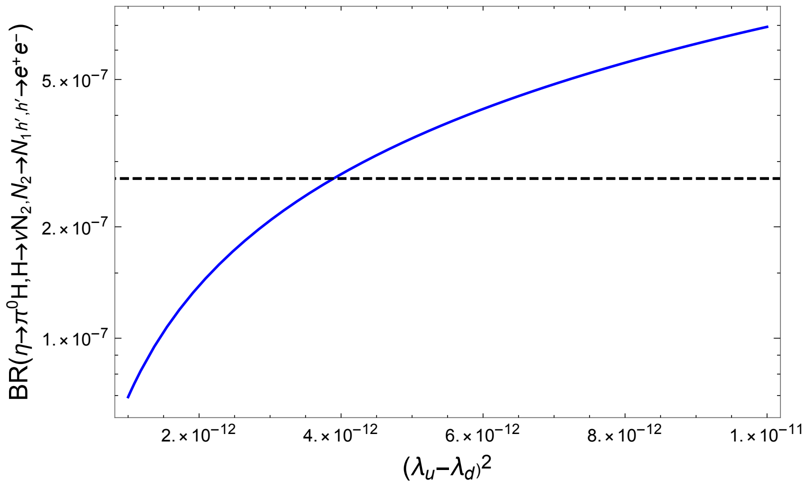

FIG. 12. Branching ratio for the process $\eta \to \pi^0 H$; $H \to \nu N_2$; $N_2 \to N_1 h'$; $h' \to e^+e^-$ predicted by the Two Higgs Doublet model [18] as a function of $(\lambda_u - \lambda_d)^2$. The dashed line corresponds to the experimental limit for REDTOP with an integrated luminosity of $3.3{\times}10^{18}$ POT.

for the π^0, all the additive quantum numbers for the η and η' are zero, and they differ from the vacuum only in terms of parity. Due to the opposite G parities of the the π^0 and η, couplings to strong interactions are suppressed. Thus, tests of C and CP in electromagnetic interactions are much more directly accessible in η and η' decays, limited mainly by the flux of such mesons [27]. In addition, such decays can provide tests of P, T, CT, PT, and even CPT. Among other possibilities are searches for lepton family violation, leptoquarks, and significant tests of the parameterization of chiral perturbation theory.

Almost all searches for symmetry violations in η/η' decays are upper limits in the range of 10^{-5} or higher [26]. Most models of symmetry violations for various decay processes are at or below the level of 10^{-9}, typically by several orders of magnitude. The number of η samples to 1.1×10^{14} and η' samples to 1×10^{12} generated at REDTOP, along with a nearly 4π detector will provide the necessary sensitivity to probe most of such models.

1. *Tests of CP symmetry*

CP violation has been extensively studied in the flavor-changing decays of the neutral K- and B-mesons. The origin of the violation is still not fully understood. The standard model predicts that the source of CP violation is a single phase in the Cabbibo-Kobayashi-Maskawa (CKM) mixing matrix of quarks couplings. At present, the predictions based on CKM mechanism are consistent with the observations in K and B systems, but tensions are arising. We propose to explore other sources of CP violation beyond the CKM mechanism and with flavor-conserving processes, especially through measurements not bound by EDM limits. Rare η/η' decays provide a good laboratory for that. All decays of the η/η' mesons into multiple photons or into photons plus π^0s provides a direct test of C invariance. Each photon in the final state, including the two from π^0 decay, has $C = -1$. Because the η has $C = +1$, final states with an odd number of photons are forbidden. However, the branching ratio for these processes are bound by EDM measurements and they would explore aspects of CP violations not accessible even at a η-factory. We propose, instead, studying three processes that are not bound by current EDM measurements and that are probing different operators which would induce a violation of CP from sources Beyond the Standard Model.

Several η/η'-related processes have been selected to study the sensitivity of REDTOP to Conservation Laws. These studies are restricted, for now, only to the CP violation (CP) and Lepton Flavor Universality, where more solid theoretical models exists which are consistent, at the same time, with bounds from EDM measurements and with outstanding experimental anomalies. These are discussed below, alongside with the theoretical models supporting them.

CP-*violation studies from Dalitz plot mirror asymmetry in* $\eta \to \pi^+\pi^-\pi^0$
The decay $\eta \to \pi^+\pi^-\pi^0$ can only occur when isospin or/and charge conjugation (C) is/are broken. Thus the interference of a C-conserving but isospin-breaking amplitude with a C-violating one would give rise to a charge asymmetry in the Dalitz plot of the 3π final state for this process. Since parity P is conserved in this decay, the existence of a nonzero charge asymmetry would attest to the breaking of C *and* CP symmetry. In contrast, searches for a nonzero permanent electric dipole moment (EDM) probe the possibility of new sources of P *and* CP violation. Moreover, the Standard Model mechanism of CP violation, vis-a-vis the flavor-changing weak interactions of quarks, is expected to be negligible in this context. Thus the measurement of the charge asymmetry in $\eta \to \pi^+\pi^-\pi^0$ decay is an ideal probe with which to explore the possibility of physics beyond the Standard Model. The REDTOP experimental concept is well suited to careful measurements of the charge asymmetry observable. Recently, theoretical work has been done [28, 29] investigating the patterns of C and CP violation in this process from mirror asymmetry breaking of the Dalitz plot. In particular, the charge asymmetry can be probed through the measurement of a left-right asymmetry of the plot [30]. Experimentally, the first measurement of such an asymmetry has been done by the KLOE Collaboration in 2009 [31]. The currently best measurement has been performed by the WASA-at-COSY Collaboration [32] and it is consistent with zero. However, the statistical error (based on the production of $3 \cdot 10^7$ η mesons from the reaction pd$\to^3$He η) largely dominated the measurement.

The matrix element generating the asymmetry in the Dalitz plot of this process, in the Gardner-Shi parametrization scheme (cf. Ref.[28]), depends on two complex parameters $\bar{\alpha}$ and $\bar{\beta}$. The statistical uncertainties for a set of parameters the Standard Model configuration see that the CP-violating parameters are all zero. are summarized in Table V. The projected sensitivities for the event sample obtained with the full integrated luminosity of 3.3×10^{18} POT (corresponding to 3×10^{10} reconstructed $\eta \to \pi^+\pi^-\pi^0$ events) are given for case of no-background and 100%-background contamination. They are much smaller than from the KLOE result and potentially sufficient to detect non-zero values of the CP-violating parameters.

Tests of CP-invariance via γ^* *polarization studies in* $\eta \to \pi^+\pi^-\gamma^*$
P and CP violation in the decay of $\eta \to \pi^+\pi^-\gamma$ has been discussed nearly fifty years

#Rec. Events	Re(α)	Im(α)	Re(β)	Im(β)	**p-value**
10^8 (no-bkg)	3.3×10^{-1}	3.7×10^{-1}	4.4×10^{-4}	5.6×10^{-4}	17%
Full stat. (no-bkg)	1.9×10^{-2}	2.1×10^{-2}	2.5×10^{-5}	3.2×10^{-5}	17%
Full stat. (100%-bkg)	2.3×10^{-2}	3.0×10^{-2}	3.5×10^{-5}	4.5×10^{-5}	16%

TABLE V. Sensitivities – statistical uncertainties for the two complex Dalitz plot CPV parameters α and β according to Ref. [28]. The generated distribution is the Standard Model configuration i.e., $\alpha, \beta = 0$. The fit reproduces the generated input, with the p-values given in the last column, within the statistical uncertainties given for the real and imaginary parts of the parameters as given in the columns 2–5.

ago [33]. A more recent study [34] has analyzed the CP-violating effects in this decay by considering the photon polarizations, and predicted that a sizable linear photon polarization could be expected in some new physics scenarios. In order to avoid measuring the photon polarization, one can consider, as shown in Ref. [35], the decay $\eta \to \pi^+\pi^-e^+e^-$ resulting from the internal conversion of the photon into an e^+e^- pair, and the CP-violating effects hidden in the polarization of the photon now can be translated into the CP asymmetry in the angular correlation of the e^+e^- plane relative to the $\pi^+\pi^-$ plane. This is actually analogous to the neutral K system, in which a large CP asymmetry, due to the interference between the parity-conserving magnetic amplitudes and the parity-violating electric amplitudes of $K_L \to \pi^+\pi^-\gamma^* \to \pi^+\pi^-e^+e^-$, has already been predicted theoretically and confirmed experimentally. Thus the asymmetry in $\eta \to \pi^+\pi^-e^+e^-$ transition could be found by analyzing its angular distribution [35], which is given by

$$A_\phi = \langle sign(\sin\phi\cos\phi)\rangle = \frac{\displaystyle\int_0^{2\pi} \frac{d\Gamma(\eta \to \pi^+\pi^-e^+e^-)}{d\phi} d\phi \; sign(\sin\phi\cos\phi)}{\displaystyle\int_0^{2\pi} \frac{d\Gamma(\eta \to \pi^+\pi^-e^+e^-)}{d\phi} d\phi}, \tag{5}$$

where ϕ is the angle between the e^+e^- and $\pi^+\pi^-$ planes in the η rest frame (see Fig. 13). It is obvious that the asymmetry in the flavor-conserving $\eta \to \pi^+\pi^-e^+e^-$ decay, different from flavoring-changing processes like $K_L \to \pi^+\pi^-e^+e^-$, indicates the presence of non-standard CP-violation. It has been shown in [34, 35] that this asymmetry will arise if a relevant parity-violating electric transition exists, and such manifestation of CP violation in some New Physics scenarios might not be bounded by existing EDM measurements; cf. however the discussion in Ref. [36].

The asymmetry defined in Eq. (5) can be expressed in terms of the the dihedral angle ϕ between the decay planes of the lepton-antilepton pair and the two charged pions.

$$A_\Phi = \frac{N(\sin\phi\cos\phi > 0) - N(\sin\phi\cos\phi < 0)}{N(\sin\phi\cos\phi > 0) + N(\sin\phi\cos\phi < 0)} \tag{6}$$

CP invariance requires A_Φ to vanish. At present, the measurement of such an asymmetry performed by the WASA-at-COSY collaboration [37] is the best available, and it is consistent with zero within the measurement errors. However, the measurement, from the production

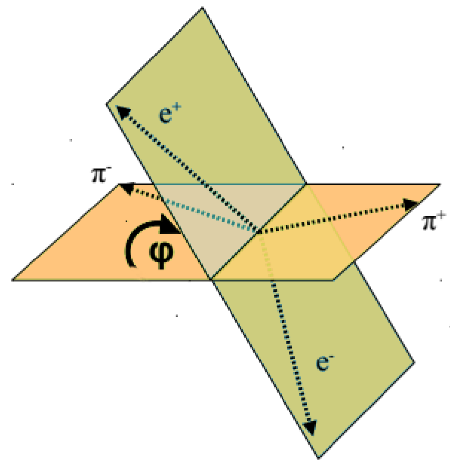

FIG. 13. Definition of the dihedral angle ϕ for the $\eta \rightarrow \pi^+\pi^-e^+e^-$ decay in rest frame of the the η meson.

of of $3 \cdot 10^7$ η mesons from the reaction pd$\rightarrow^3$Heη, is largely dominated by the statistical error.

The asymmetry for REDTOP has been estimated using a reduced data sample corresponding to 2×10^{-5} of the full sample proposed. The curve is plotted in Fig. 14 vs the true value for five different values of A_Φ. The diluting effect of the background is clearly

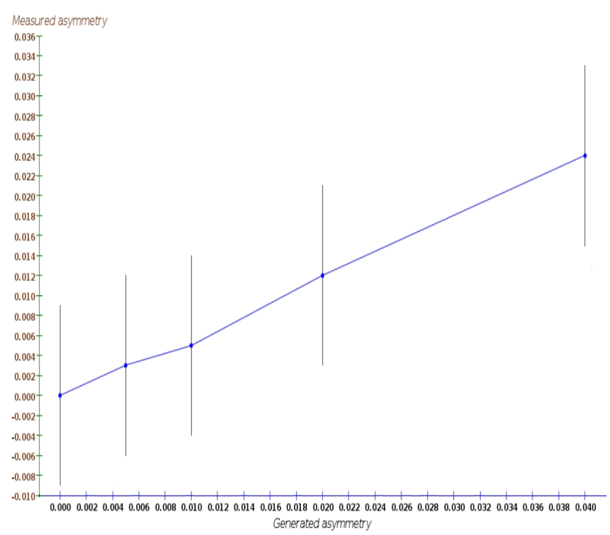

FIG. 14. Sensitivity to $sin\phi cos\phi$ asymmetry for $\eta \rightarrow \pi^+\pi^-e^+e^-$. The errors in the plot are statistical only.

observed since the measured asymmetry is reduced by a factor of $\sim$65% wrt the true value. We conclude that the measured asymmetry for the samples considered is larger than the statistical error (which is the dominant component in the measurements by WASA and

KLOE experiments) for values of the true asymmetry larger than approximately 1×10^{-2}. When the total integrated luminosity of 3.3×10^{18} POT foreseen for REDTOP is taken into account, we expect that the statistical error will be reduced by at least two orders of magnitude, corresponding to a contribution to the A_ϕ sensitivity smaller than $\sim 10^{-4}$. We conclude that the uncertainty on the measured asymmetry will be dominated by the systematic error.

T*ests of CP-invariance with double Dalitz decays* $\eta \to \ell^+\ell^-\ell'^+\ell'^-$
Similar to $\eta \to \mu^+\mu^-$ decays, CP violation effects arise trough hadronic operators driving CP-odd transition form factor [38]. In particular, the contribution to the asymmetry in the dihedral angle can be expressed as

$$A_{\sin\phi\cos\phi} = \mathrm{Im}[1.9c^{2222}_{\ell edq} - 1.3(c^{(1)2211}_{\ell equ} + c^{1122}_{\ell edq})] \times 10^{-5} - 0.2\epsilon_1 + 0.0003\epsilon_2 \tag{7}$$

where $c_{\mathcal{O}}$ are the corresponding Wilson coefficients [5] characterizing the coupling strength of the CP-violating TFFs. Testing CP-violation in pseudoscalar mesons via a search for asymmetries in double Dalitz decays has the advantage that it does not require to measure the polarization of the leptons. The estimated asymmetries for REDTOP for a reduced data sample corresponding to 10^4 of the full proposed sample are plotted in Fig. 15 vs the Monte Carlo generated value. When extrapolating the results to the full integrated

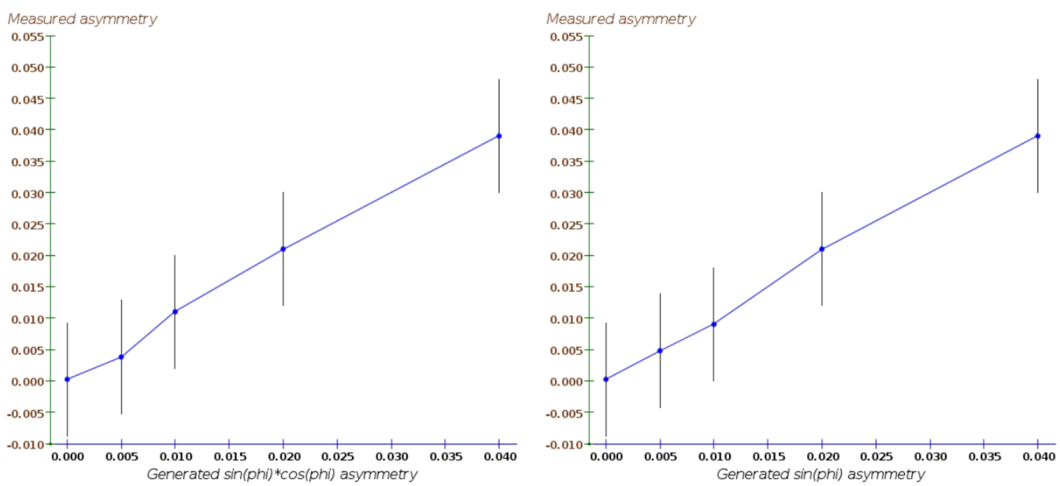

FIG. 15. Sensitivity to $sin\varphi cos\varphi$ (left) and $sin\varphi$ (right) asymmetries for $\eta \to \mu^+\mu^-e^+e^-$.

luminosity of 3.3×10^{18} POT foreseen for REDTOP, we estimate that the statistical error will be reduced by about than two orders of magnitude, corresponding to a contribution to the sensitivity smaller than $\simeq 10^{-4}$. Therefore, we conclude that the uncertainty on the measured asymmetry will, most likely, be dominated by the systematic error. Using the results above, we obtain the following sensitivities for the CP-violating Wilson coefficients:

$$\Delta c^{2222}_{\ell edq} = 8, \quad \Delta c^{2222}_{\ell edq} = 5, \quad \Delta\epsilon_1 = 5 \times 10^{-4}, \quad \Delta\epsilon_2 = 0.3. \tag{8}$$

2. Tests of Lepton Flavor Universality

Another set of potential probes of high-energy New Physics are ratios of η or η' decays to $X\ell^+\ell^-$, where ℓ is different between the numerator and the denominator and X denotes additional final-state particle(s). Such ratios would probe lepton universality. A few considerations are in order however. First, decays induced by the weak interaction are extremely rare, below 10^{-10}, and thus well below, by many orders of magnitude, existing experimental upper limits. The purely leptonic case is, as mentioned, dominated by intermediate di-photon exchange, and the suppression of this SM mechanism would suggest these decays as good probes of BSM effects. Handy formulae can be found in Ref. [36]. As a consequence, again, these ratios are way more suited as probes of light, GeV-scale or below, New Physics.

From the experimental point of view, leptonic and semileptonic decays of the η mesons have relatively clear signatures in REDTOP, and they can be disentangled with good efficiency, from the large hadronic background. Furthermore, the decay rate into electrons and muons are only slightly affected by the different phase space. Therefore, those decays represent an excellent opportunity to probe Lepton Flavor Universality (LFU). To estimate REDTOP sensitivity to LFU, we have considered two groups of processes: $\eta \to \ell_1\bar{\ell}_1\ell_2\bar{\ell}_2$, and $\eta \to \gamma\ell\bar{\ell}$.

$\eta \to 4\,leptons$ decays

Only the decays of the $\eta \to e^+e^-e^+e^-$ has been experimentally observed, with a measured branching ratio of 2.4×10^{-5} [39], corresponding to an expected yield at REDTOP of 2.6×10^9 produced events. An estimate for the other two processes can be made following Ref. [40], for which we foresee a yield of order $\mathcal{O}(10^7)$ and $\mathcal{O}(10^4)$, respectively, for the $\eta \to e^+e^-\mu^+\mu^-$ and $\eta \to \mu^+\mu^-\mu^+\mu^-$ decays. The studies performed on these processes have been carried using different η-meson samples. The corresponding POT are summarized in the second column of Table VI. Details of the Montecarlo study can be found in reference [5].

The statistical errors on the branching ratios obtained from the fit to to the invariant mass of the four leptons for each final state considered are summarized in Table. VI. When

Process	POT	Signal events	**Statistical error**
$\eta\to e^+e^-e^+e^-$	4.4×10^{14}	53,934	**0.5%**
$\eta\to e^+e^-\mu^+\mu^-$	1.6×10^{15}	18,841	**0.8%**
$\eta\to \mu^+\mu^-\mu^+\mu^-$	2.2×10^{18}	10,548	**1.0%**

TABLE VI. Statistical error from the fit of $\eta \to 4\,leptons$ and Urqmd generated background using a gaussian and a 5th-order polynomial. The POT corresponding to each data sample is indicated in the second column.

the statistics of the full event sample is taken into account, the projected statistical error for the two processes with electrons in the final state is expected to be of the order of 10^{-5}.

$\eta \to \gamma\ lepton - antilepton\ decays$

The presence of the additional photon in this case implies additional SM contributions, but the main conclusions reached in the purely leptonic case still hold. One important feature of the radiative 2-leptons case with respect to the non-radiative counterpart is the fact that the chiral suppression inherent in the latter decay [41] is lifted because of the additional photon. Ratios of radiative di-leptonic decay rates, where the numerator and the denominator only differ by the lepton flavour are then excellent tests of Lepton Universality [42], and, by the previous argument, they are expected to be very close to unity within the Standard Model.

The studies performed on these processes are based on a relatively small η-meson sample consisting of 4.65 $\times 10^6$ events. That sample corresponds to $\sim 4 \times 10^{-8}$ of the integrated luminosity foreseen for the experiment. The statistical errors on the branching ratio were obtained from the fit to the invariant mass of the $\eta \rightarrow \gamma\ lepton - antilepton$ system for each final state considered. They are shown in Table. VII

Process	POT	Signal events	Background events	$\frac{S}{\sqrt{B}}$	**Statistical error**
$\eta \rightarrow \gamma\, e^+e^-$	1.38×10^{11}	2.13×10^6	2.52×10^4	1.3×10^4	**0.09%**
$\eta \rightarrow \gamma\, \mu^+\mu^-$	1.38×10^{11}	8.84×10^5	6.5×10^3	3.5×10^3	**0.14%**

TABLE VII. Statistical error from the fit of $\eta \rightarrow \gamma\ lepton - antilepton$ and Urqmd generated background using a gaussian and a 5th-order polynomial, for 1.38×10^{18} POT

When the statistics of the full event sample for 3.3×10^{18} POT is taken into account, the projected statistical error for the $\eta \rightarrow \gamma\ lepton - antilepton$ final state is expected to be of the order of 10^{-6}, certainly negligible compared to the systematic error.

3. *Remarks on Lepton Flavor Universality measurements with η mesons*

The theoretical discussion about the REDTOP sensitivity to LFU measurements deserves some further qualifications. As well-known, LFU measurements have recently come to the fore because of a coherent array of discrepancies in measurements of semi-leptonic $b \rightarrow s$ and $b \rightarrow c$ decays at LHCb and B factories. The natural question is whether the putative beyond-SM LFU that these discrepancies imply could be tested in decays of light mesons, e.g. kaons [43], and the $\eta^{(\prime)}$. On the latter there is a conspicuous gap in the literature, and on the other hand this possibility would be an important physics case for REDTOP. We would like to bring the attention on the following two points.

The first point is the fact that LHCb and B factories access decays that directly probe—by definition—the operators affected by the putative B anomalies, i.e., 4-fermion structures of the kind $(\bar{s}\Gamma b)(\bar{\ell}\Gamma'\ell)$, where Γ, Γ' denote appropriate strings of Dirac matrices, and ℓ is any of the charged leptons. Conversely, in the case of $\eta^{(\prime)}$ we access operators with quarks (and leptons) of the light generations only. Relating the different quark sectors requires assumptions on the flavor structure of the couplings, and the suppression is "by default" CKM-like (see e.g. [44]).

The second point is that $\eta^{(\prime)}$ leptonic decays are dominated by the (long-distance) contribution with two intermediate photons. As a consequence, in order to have sensitivity to new physics, the latter must give a signal unambiguously larger than the uncertainty associated with such long-distance contribution. This makes these decays way more suited as probes of *light*, MeV–GeV-scale new physics. This happens to be a very active field of research currently (see e.g. [45] for a recent review), and has even been considered as a solution of B anomalies [46–53].

C. Muon polarimetry at REDTOP

A striking consequence of the quantum numbers of the η/η' mesons is that, for selected decays, certain net muon polarizations, such as longitudinal or transverse, are highly suppressed in the SM. This opens the door for exploration of a broad range of NP effects which would become manifest with a non-null polarization of the muons obtained from the decay of the η/η' mesons. The theory behind two example channels for BSM searches enabled by a muon polarimeter at REDTOP are discussed below. More details could be found in reference [5].

Muon polarimetry is based on the measurement of the shape of the positron (electron) spectrum from $\mu \to e\nu_\mu\bar{\nu}_e$ decay in flight, which depends on the polarization of the parent muon. To study muon polarimetry a detector must meet the following three requirements: a) the detector has to be made of a material which does not change the initial polarization of the muon, b) the detector granularity has to be sufficiently small to be able to measure the angle between the path of the decaying muon and the electron, and c) the detector must have a magnetic field of precisely known intensity to measure the momentum of the leptons.

The implementation of muon polarimetry is currently under study at REDTOP by exploiting two options. In the first option, The ADRIANO2(3) calorimeters will be used (see also Sec. V E), possibly instrumented with a few layers with smaller tiles to increase the granularity in the region where muon polarimetry is performed. The material used for ADRIANO2 tiles (lead glass and scintillating plastic) is amorphous and it will not change the original polarization of the muon, as it will occur, for example, with crystal calorimeters. Since the calorimeter will be immersed in a 0.6 T uniform magnetic field, all three requirements for polarimtry will be met. In the second option, a dedicated polarimeter will be inserted approximately 20 radiation lengths inside the calorimeter. The polarimeter would be made of thick aluminum plates, where the muon will either stop or decay in flight, interspersed with gaseous tracking chambers which will detect the electron. Aluminum will not affect the original polarization of the muon.

1. *CP violation via transverse or longitudinal muon polarization*

The muon pair in $\eta \to \mu^+\mu^- X$ decays can be produced in a $^1S_0$ or a $^3P_0$ state, the former corresponding to a CP-conserving transition and the latter to a CP-violating one.

The most general structure has the form given in Eq. (9).

$$\mathcal{M} = g_P(\bar{u}i\gamma^5 v) + g_S(\bar{u}v), \tag{9}$$

with $g_{P,S}$ dimensionless parameters. Both contributions are C even, while $g_{P,S}$ terms are P even and P odd, respectively. The polarized decay width can be expressed as [38]

$$d\Gamma = \frac{\beta_\mu}{16\pi m_\eta} \times \frac{m_\eta^2}{2}\Big[|g_P|^2(1 - s^+\cdot s^-) + |g_S|^2\beta_\mu^2[1 - \{2(s^+\cdot\hat{\boldsymbol{\beta}}_{\mu^+})(s^-\cdot\hat{\boldsymbol{\beta}}_{\mu^+}) - s^+\cdot s^-\}] \\ + 2\,\mathrm{Re}(g_P g_S^*)\boldsymbol{\beta}_{\mu^+}\cdot(s^-\times s^+) + 2\,\mathrm{Im}(g_P g_S^*)\boldsymbol{\beta}_{\mu^+}\cdot(s^+ - s^-)\Big], \tag{10}$$

where $\boldsymbol{\beta}_{\mu^+}$ is the μ^+ velocity, with modulus $\beta_\mu = (1-4m_\mu^2/m_\eta^2)^{1/2}$, and $s^\pm$ stands for the $\mu^\pm$ spin(see [38, 54] and references therein). The expression above allows for an easy connection to the spin density formalism (see Ref. [55]) upon $s \to \tau$.

This decay allows for tests of CP violation via longitudinal and transverse spin polarizations, defined as

$$P_L = \frac{N_R - N_L}{N_R + N_L} \qquad P_T = \frac{N_{RH} - N_{LH}}{N_{RH} + N_{LH}}, \tag{11}$$

with $N_{R(L)}$ counting the numbers of outgoing μ^+ with positive(negative) helicity and $N_{RH(LH)} = (s^+\times s^-)\cdot\boldsymbol{\beta}_{\mu^+}$ positive(negative). We note that P_L is of the C even, P odd, T even kind, while P_T is of the C even, P odd and T odd kind. Therefore, both polarizations probe CP violation.

Any source of CP violation in these decays would clearly point to NP since, in the SM, CP violation requires the presence of the CKM matrix and thus electroweak physics, necessarily involving weak and CKM suppression factors. At REDTOP, three processes have been considered and the sensitivity to CP violation has been estimated. In the studies, we have assumed a conservative value for the reconstruction efficiency of the muon decay $\epsilon_{\rm pol} = 50\%$ estimate both for signal and background. They are discussed briefly in the following paragraphs. More details can be found in reference [5];

CP violation in $\eta \to \mu^+\mu^-$ decays

The most general amplitude for $\eta \to \ell^+\ell^-$ can be effectively parametrized as with $g_{P,S}$ dimensionless parameters. The first contribution is CP even and has been computed in the Standard Model (see [38, 54] and references therein), while the latter represents a P-odd C-even contribution, that is negligible in the Standard Model. As such, any indication of a nonzero g_S would be a clear signal of New Physics. Ref. [38] introduced two different muon's polarization asymmetries, directly related to the experimental measurements defined in Eq. (11) :

$$A_L = \frac{N(\cos\theta > 0) - N(\cos\theta < 0)}{N} = \mathrm{Im}[4.1c_{\ell edq}^{2222} - 2.7(c_{\ell equ}^{(1)2211} + c_{\ell edq}^{2211})] \times 10^{-2}, \tag{12}$$

$$A_\times = \frac{N(\sin\Phi > 0) - N(\sin\Phi < 0)}{N} = \mathrm{Im}[2.5c_{\ell edq}^{2222} - 1.6(c_{\ell equ}^{(1)2211} + c_{\ell edq}^{2211})] \times 10^{-3}, \tag{13}$$

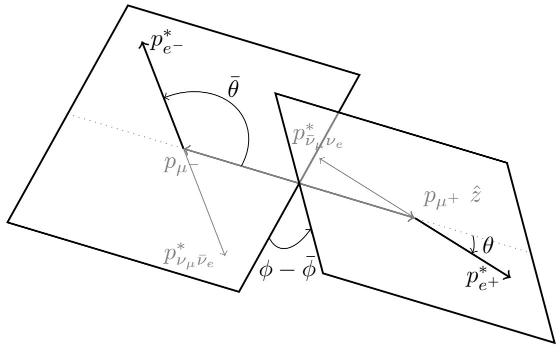

FIG. 16. Kinematics of the process. The decaying muons' momenta in the η rest frame are noted as $p_{\mu^\pm}$, while the $e^\pm$ momenta, $p^*_{e^\pm}$, is shown in the corresponding $\mu^\pm$ reference frame along with the momenta of the $\nu\bar{\nu}$ system. The $\hat{z}$ axis is chosen along p_{μ^+}.

Above, θ represents the polar angle of the e^+ in the μ^+ reference frame, with the $\hat{z}$ axis fixed by the μ^+ direction in the η rest frame, see Fig. 16. The angle $\Phi = \phi - \bar{\phi}$ is defined in Fig. 16 and reflects the sign of $(\vec{p}_{e^-} \times \vec{p}_{e^+}) \cdot \vec{p}_{\mu^+}$. The right hand side in the equation above provides the contribution from the aforementioned operators, with $c_{\mathcal{O}}^{(llqq)}$ the corresponding Wilson coefficient for the $l(q)$-th lepton(quark) generation, respectively. The sensitivity to the Wilson coefficients is derived through the asymmetries in Eqs. (12, 13) and will be limited by the statistical error on the signal diluted by the background. Combining them and assuming a conservative $\epsilon_{\mathrm{pol}} = 50\%$ estimate both for signal and background, we derived the statistical error for $(A_L$:

$$\Delta(A_L) = \frac{\sqrt{N}_{\eta\to\mu^+\mu^-} + \sqrt{N}_{\mathrm{bkg}}}{N_{\eta\,\to\,\mu^+\mu^-}} = 2.7 \times 10^{-3}. \tag{14}$$

Comparing to Eq. (12), we obtain for the full data sample foreseen for REDTOP, the following estimate for the Wilson coefficients:

$$\Delta(c^{1122}_{\ell equ}) = 0.1 \times 10^{-1}, \quad \Delta(c^{1122}_{\ell edq}) = 0.1, \quad \Delta(c^{2222}_{\ell edq}) = 6.6 \times 10^{-2}, \tag{15}$$

that for the $c^{2222}_{\ell edq}$ coefficient corresponds to the same order of precision obtained from nEDM bounds.

CP violation in $\eta \to \pi^0\mu^+\mu^-$ decays

The $\eta \to \pi^0\mu^+\mu^-$ process is a great testing ground for BSM searches, such as, for example, P-odd, C-even new-physics effects. In particular, with 3 particles in the final state, this necessarily involves polarization observables, in line with $\eta \to \mu^+\mu^-$ decays, see Sect. (III C 1). The possibility of testing P-odd, C-even contributions was studied in Ref. [56] using the SMEFT as the general framework to capture physics BSM. Once again, the key polarisation observables are those defined in Eqs. (12, 13). Using input from Ref. [12], the asymmetries can be written as:

$$A_L^{\eta\to\pi^0\mu^+\mu^-} = -0.19(6)\,\mathrm{Im}\,c_{\ell equ}^{(1)2211} - 0.19(6)\,\mathrm{Im}\,c_{\ell edq}^{2211} - 0.020(9)\,\mathrm{Im}\,c_{\ell edq}^{2222}\,, \tag{16}$$

$$A_\times^{\eta\to\pi^0\mu^+\mu^-} = 0.07(2)\,\mathrm{Im}\,c_{\ell equ}^{(1)2211} + 0.07(2)\,\mathrm{Im}\,c_{\ell edq}^{2211} + 7(3)\times 10^{-3}\,\mathrm{Im}\,c_{\ell edq}^{2222}\,. \tag{17}$$

The comparatively larger suppression for the s-quark contribution arises from isospin breaking, that is an $\mathcal{O}(1\%)$ effect, and reduces the sensitivity as compared to $\eta\to\mu^+\mu^-$ decays. Current nEDM bounds imply for the above asymmetries that $A_L < 4\times 10^{-4}$ and $A_\times < 1.4\times 10^{-4}$, which should be contrasted with the REDTOP capabilities.

The sensitivity to the Wilson coefficients is derived through the most sensitive asymmetry, Eq. (16), that will be limited by statistical error on the signal diluted by the background. From a Montecarlo analysis on this process, we expect for the statistical error:

$$\Delta(A_L) = \frac{\sqrt{N}_{\eta\,\to\,\pi^0\mu^+\mu^-} + \sqrt{N}_{\mathrm{bkg}}}{N_{\eta\,\to\,\mu^+\mu^-}} = 4.0. \tag{18}$$

where we have assumed a conservative $\epsilon_{\mathrm{pol}} = 50\%$ estimate both for signal and background. Comparing to Eq. (16), we find, for the Wilson coefficients responsible for the asymmetries, the following sensitivities:

$$\Delta(c_{\ell equ}^{1122}) = 21, \quad \Delta(c_{\ell edq}^{1122}) = 21, \quad \Delta(c_{\ell edq}^{2222}) = 200. \tag{19}$$

CP-*violation in the decays* $\eta\to\gamma\mu^+\mu^-$

The sensitivity to this process is studied by measuring the polarization of the muons reconstructed from the $\eta\to\gamma\mu^+\mu^-$ decay. The relevant observable is the asymmetry defined in Eq.(16), which carry the information from the muon polarization. The study is conducted in a similar fashion as that described in Sec. III C 1. Assuming a conservative $\epsilon_{\mathrm{pol}} = 50\%$ estimate both for signal and background, we obtain $\Delta(A_L) = 1.4\times 10^{-5}$. The sensitivities for the corresponding Wilson coefficients are:

$$\Delta(c_{\ell equ}^{1122}) = 2.6, \quad \Delta(c_{\ell edq}^{1122}) = 2.6, \quad \Delta(c_{\ell edq}^{2222}) = 1.7. \tag{20}$$

2. *CPT violation in transverse polarization*

As noted in the previous section, the transverse muon polarization P_T in meson decays is a T-odd observable, defined by the projection of the $\mu^\pm$ spin transverse to the decay plane. A non-zero value of P_T would be a clear evidence for violation of time reversal invariance (T) [57], since the spurious effects from final state interactions are small [58].

Violation of time reversal symmetry (T) provides an alternative means to search for violation of charge conjugation and parity (CP) based on the more general CPT theorem. Sources of CP violation beyond the SM in the neutral meson sector are one of Sakharov's criteria [57] for an explanation of the matter-antimatter asymmetry observed in the universe.

Electroweak theory allows one to link T-odd observables (which change sign under time reversal transformation) to time reversal symmetry breaking, which can be interpreted as a clear indication of NP. The transverse polarization P_T of muons in η/η' decays is depicted in Fig. 17 for Dalitz (left) and semileptonic (right) decays.

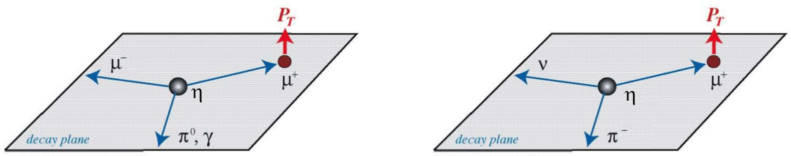

FIG. 17. Transverse muon polarization P_T in Dalitz (left) and semileptonic (right) η decays at rest.

The SM prediction for P_T is extremely small, arising only from higher-order loop contributions [59]. As an example, these have been computed in the context of kaon decays [58, 60], finding them at the 10^{-5} level — similar results should apply to $\eta \to \pi^-\mu^+\nu$ decays. More complex models involving NP such as multi-Higgs doublet models, leptoquark models or supersymmetric models with R-parity breaking or s-quark mixing predict much larger values for P_T ranging from 10^{-4} to 10^{-2} [61, 62]. As a side note, the $\eta \to \pi\mu\nu_\mu$ process has not been observed yet.

In Dalitz decays, $\eta \to \gamma\ell^+\ell^-$, the leading order QED and weak contributions do not contribute to such an asymmetry [38], such that any positive observation at REDTOP would correspond to BSM physics. Likewise, in $\eta \to \pi^0\mu^+\mu^-$, no contribution to such an asymmetry was found in [56], such that any positive finding would point to BSM physics. In conclusion, any observation of a transverse muon polarization in the 3-body decays of η/η' mesons is an unambiguous indication of CPT violation and BSM physics.

D. Non-perturbative QCD

Studying the decays of η and η' mesons open a window into the complex QCD dynamics at low energies. For recent reviews on the subject, see e.g. [36, 63]. At these energies, ($m_\eta \sim 548$ MeV and $m_{\eta'} \sim 958$ MeV) strong interactions become non-perturbative and the usual series expansion in the strong coupling constant does not provide an appropriate theoretical framework. One has to instead rely on non-perturbative techniques such as effective field theory—Chiral Perturbation Theory (χPT) for light quarks—, dispersion relations, or numerical simulations such as lattice QCD. The η meson is very peculiar: its main decay channel $\eta \to 3\pi$ violates G-parity, thereby providing an unique access to the light quark masses. It also allows one to test the χPT framework and complement it with the dispersive methods. The description of η' decays poses additional challenges. In particular, it requires an extension of the χPT framework, many aspects of which still remain to be worked out.

The REDTOP experiment with the expected 10^{14} η and 10^{12} η' will provide crucial data to advance this endeavor to the next level of precision.

IV. EXPERIMENTAL SITUATION

Although there are efforts underway and planned to collect η/η' mesons, in all cases either the statistics or the backgrounds will significantly limit sensitivity relative to REDTOP. The present η/η' data sample, consisting of $\sim 10^{10}$ collected mesons, is entirely dominated by the WASA and KLOE experiments with $\sim 10^{9}$ each. The KLOE sample, obtained from the radiative decay of the Φ mesons, is fully tagged, and has a larger S/B compared to WASA. Unfortunately, the KLOE detector is sensitive to new particles with a mass larger than $\sim 50\,\mathrm{MeV}$, which misses, for example, the range around $17\,\mathrm{MeV}$ of interest for the exploration of the Atomki anomaly [64].

CMS has recently initiated a search for NP in the MeV-GeV range (see, for example, ref. [65]) with $\sim 5 \times 10^{12} (\sim 1 \times 10^{12})$ η/η' collected in Run-2. Despite the large sample, the S/B obtained with 13 TeV protons is ~ 200 times worse than that observed with a 1.8 GeV beam, reducing considerably the sensitivity of the LHC experiments to NP in the MeV-GeV mass range.

A large source of tagged η/η' mesons foreseen in the next decade would come from the Super Tau-Charm Factory (STCF), currently proposed in Hefei, China. With a peak luminosity of more than $0.5 \times 10^{35} cm^{-2}/s$, the STCF is expected to increase the BES-III η/η' sample by a factor of about 100, corresponding to $\simeq 6 \times 10^{9}/year$[66]. These statistics are still four orders of magnitude lower than that foreseen for REDTOP. If STCF is approved, construction of the accelerator could begin in 2026, while operations would start about five years later. REDTOP has a similar timeline with the advantage of requiring no new accelerator construction (if running at the SIS18).

A hypernuclei spectrometer is currently being proposed to run at the new HIAF laboratory in Huizhou, China. Although the detector is not optimized for η physics, the energy and intensity of the beam (interaction rate $\simeq 100 MHz$) are close to those proposed by REDTOP ($\simeq 500 - 700$ MHz). Therefore, the experiment will produce a number of mesons adequate to explore NP. Detector optimization and physics sensitivity studies are under way. A collaborative effort between the two collaborations is under discussion.

The High-Luminosity upgrade of the LHC will increase the production of η/η' mesons by one order of magnitude, in line with that foreseen for REDTOP. However, the S/B ratio is not expected to improve appreciably. Therefore, LHC sensitivity remain below that of a dedicated η/η'-factory.

V. THE REDTOP EXPERIMENT

A. The experimental concept and detector requirements

The most efficient production method of η/η' mesons is from nuclear scattering of a proton or pion beam onto a nuclear target. Despite the relatively large η/η' production cross section (see Sec. V B) the inelastic hadronic events are produced at two orders of magnitude larger probability. Consequently, rejecting that background represents the biggest challenge for the experiment. In order to achieve that, one can take advantage of the fact that most final states of interest for NP exploration contain two leptons or two (oppositely charged) pions, one of which has relatively high momentum.

The largest background component consists of events with only baryons (nucleons or ions) or a single pion. Therefore, the most critical requirement for REDTOP is excellent particle identification, optimized for baryon-lepton separation. Eventual combinatorics or particle mis-identification can be reduced with a kinematic analysis, which benefits from good energy and momentum resolution. The second largest background component derives from photons converting in the target or in the layers of the tracking system. The rejection of such background can be achieved with kinematic cuts and/or by successfully identifying a secondary vertex. Virtual photon conversion, another relevant source of background affecting mostly the search for NP with masses below 100 MeV, is being simulated by the URQMD-based event generator. Our studies indicate that it can be drastically reduced by kinematic considerations, provided that energy and momentum resolutions are sufficiently high. Good energy and momentum resolution of reconstructed particles is also important for bump-hunt analyses of final states with intermediate resonances (which includes the η/η' mesons).

One goal of the experiment is to explore NP in the mass region where the Atomki anomaly has been observed [64]. Consequently, the detector has been designed with good sensitivity to low-mass resonances, as low as 17 MeV. The η/η' mesons produced at REDTOP are almost at rest in the lab frame, experiencing a small boost in momentum of only ∼200 MeV in the direction of the incoming beam. Their momentum spectrum is almost independent of beam energies in the [1.46-2.1] GeV range. Therefore, the REDTOP detector must be hermetic, with layout similar to those typically designed for collider experiments. As a final remark, a clear indication of NP will be observation of events with a detached vertex that do not originate from the very few produced K_{short} mesons. A vertex detector is, therefore, a key component of the REDTOP experiment.

The beam and target systems and the calorimeter, tracking, and particle identification detector systems are discussed in more detail in the following sections. The detector requirements to achieve the required level of background rejection are summarized in Table VIII.

B. Hadro-production of η mesons

Above the production threshold of η/η' mesons ($E_{kin} \approx 1.2$ GeV) several intra-nuclear baryonic resonances are formed (Δ's, N(1440), N(1535), etc.), some of which decay into an η/η'-meson. The cross section for such processes increases rapidly above threshold (see left plot in Figure 18), and is about seven times larger in $p-n$ collisions than $p-p$ ones. Therefore the nuclear target should have a large neutron to proton ratio. A target with *low-Z* minimizes the formation of nuclear fragmentation products, and helps to reduce the particle multiplicity of the final state.

TABLE VIII. REDTOP detector requirements.

Measurement	performance
EM Calorimeter energy	$\sigma_E/E < 2\%/\sqrt{E} \oplus 0.3\%$
Had Calorimeter energy	$\sigma_E/E < 30\%/\sqrt{E} \oplus 5\%$
Charged track P_T	$\sigma_{P_T}/P_T^2 \sim 2 \times 10^{-3}$ GeV^{-1} for P$_T$=1 GeV
Vertex resolution	<20 μm
PID purity for e^+/e^-	>98%
PID purity for μ^+/μ^-	>95%
PID purity for π^+/π^-	>95%
PID purity for proton	>99.5%
PID purity for γ	>99%
PID purity for neutron	>99%

Extensive studies have been conducted with the *GenieHad* [67] event-generator framework using multiple beam and target parameters. Figure 18 shows *GenieHad* predictions for beam energy dependence of the total $p + Li$ inelastic cross section (left) and the probability to produce an η (right). Above threshold, the total η/η' production cross section increases approximately linearly with beam energy. The resonant production mechanism makes the momentum of the η/η' mesons in the lab frame only slightly dependent on the beam energy. The cross section in case of $p + Be$ scattering is approximately 15% larger, while the η/η' production rate is nearly unchanged. Therefore, a proton beam with E$_{kin}$ $\approx$ 1.8(4) GeV impinging on a thin, low-Z, high-A/Z material like Beryllium or Lithium is an optimal choice for the η/η' experimental program. Incidentally, we observe that the η production rate increases almost seven-fold during the η' run at 4 GeV, expanding even further the collected sample.

No experimental data on the $p - Li(Be)$ inelastic cross section nor η/η' production exist in the energy range of interest for REDTOP. To minimize the uncertainty in estimating the η/η' production cross section, we used several nuclear models in *GenieHad* to calculate the cross section and compared several nuclear transport models to describe the evolution of proton-nucleus collisions. The average values expected at REDTOP for the η/η' yields and of total nuclear inelastic interaction are summarized in Table IX .

TABLE IX. Expected η and η' yield at REDTOP for 10^{18} POT (see reference [5] for details on the estimation method)

	Expected yield for E_{kin}=1.8 GeV
N_η	5.1×10^{13}
$N_{\eta'}$	0
N_{ni}	7×10^{15}

	Expected yield E_{kin}=3.6 GeV
N_η	1.8×10^{14}
$N_{\eta'}$	2.4×10^{11}
N_{ni}	9.7×10^{15}

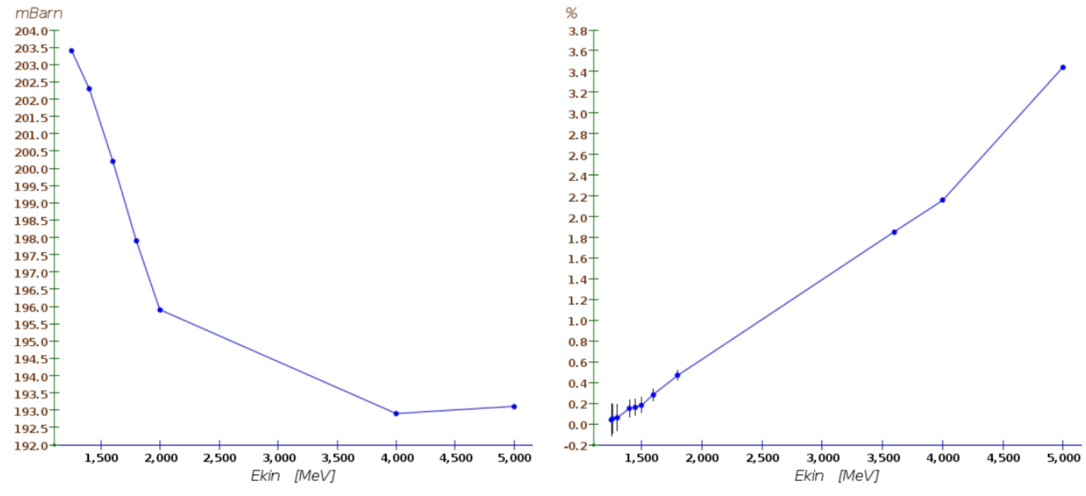

FIG. 18. Predictions of $p + Li$ cross sections versus beam energy from the *GenieHad* [67] model with Urqmd +Abla07 scattering models using the Tripathi parametrization for the inelastic cross section. The left panel shows the inelastic cross section while the right panel shows the percentage of such collisions that produce an η meson.

C. Beam and target requirements

As discussed in Sec. V B, *low-Z* nuclei with higher $^{A}/_{Z}$, makes it an ideal material for REDTOP target systems. Deuterium, Lithium, and Beryllium are currently under consideration. A study with *GenieHad-Urqmd* indicates that the multiplicity of primary particles generated in p-Li scattering at 1.8 GeV for events without an η is about 3.5 for charged (mostly, protons and pions) and 2.1 for neutral particles (3.8 charged and 3.0 neutral in Be). In order to minimize the rescattering of the η/η' decay products inside the target, the latter is split in multiple thinner foils, which also improves the measurement of the z-coordinate of the production vertex and the disentangling of overlapping events.

In conclusion, a CW proton beam delivering 1×10^{11} POT/sec on multiple foils of Li (Be) with total thickness of 7.7 (2.3) mm would generate a rate of inelastic interactions of about 700 MHz and a η-meson yield of $5.1 \times 10^{6} \eta/sec$ (cfr. Table IX), corresponding to $5.1 \times 10^{13}\, \eta/yr$.[1] The beam power corresponding to the above parameters is approx. 30 W, of which 1% (or 300 mW) is absorbed in the target systems.

D. Beam options at GSI/FAIR

There exist several options for installation of the REDTOP at GSI/FAIR which depend on the overall progress in the R&D of the REDTOP detector components folded with the timeline of the FAIR construction.

[1] Here we assume that a running time of 1-year corresponds to 10^{7} sec

Extracted beam –SIS18 Running REDTOP at an extracted beam has been studied extensively for the Snowmass-2021 study program.

The simplest option would be to employ a direct proton beam from the SIS-18. For this purpose, few locations are under consideration to transport the highest rigidity SIS-18 beams and no significant upgrades would be required.

Also the option to use direct proton beams from the SIS-100 could be considered, where REDTOP can be accommodated, e.g. in the antiproton-separator hall in case the antiproton program is further delayed.

In-ring beam –ESR/HESR The advantage of the in-ring configuration is that, assuming $\mathcal{O}(10^{10})$ protons stored in the ESR, the beam-target interaction rate would be as high as $\sim 10^{16}$ POT/s, exceeding REDTOP requirements by a factor $\sim 10^5$. The disadvantages are that a relatively thick target, required to reach the desired luminosity, would reduce the lifetime of the beam below the ring refill rate. Assuming a minimum beam lifetime of 1 s and minimum beam-target inelastic interaction rate of $\sim 100\,\mathrm{MHz}$, the proton-nucleus interaction probability (which depends on beam-target geometrical factors as well as on the inelastic cross section) must be within the range $[5 \times 10^{-9}, 3 \times 10^{-7}]$, limiting severely the options for a satisfactory target. Further, in order to install REDTOP into the ESR, the re-design of the target area will be required. Also dedicated beam optics will need to be developed to fit the injected beam into the small aperture of the REDTOP detector. REDTOP will occupy most of the target section and limit the momentum acceptance of the ESR so that running other experiments at the ESR will probably be impossible, including the ones requiring decelerated beams.

The timeline of the experiment is also consistent with running REDTOP at the High-Energy Storage Ring (HESR) of FAIR. An advantage of the HESR in comparison to the ESR (maximal magnetic rigidity Bρ(ESR)=10 Tm) is that stochastically cooled proton beams will be available at all energies up to the maximal proton energy of 14 GeV (Bρ(HESR)=50 Tm). Within PANDA project, the beam-optics of the HESR is pre-designed for having a focused beam on PANDA target, which can be explored for REDTOP. Such ion-optical mode is not presently available at the ESR. Furthermore, the 574-m long HESR offers more space for installing REDTOP experiment as the 108-m long ESR.

The installation of REDTOP at HESR depends on the timeline for delivering antiproton beams to PANDA. The REDTOP detector can be installed in the long straight section in the electron cooler building or in the PANDA detector station. The latter option has the advantage that the ion-optics of the HESR are designed for an efficient collision zone there. whether the HESR lattice can enable a similar focus on the opposite side of PANDA will require study.

In conclusion, while the in-ring configuration is very promising, more studies must be carried over before the design of the experiment could be finalized.

Conclusion The collaboration is open to any beam option, although the extracted beam (SIS18) has been studied in great detail and the sensitivity to BSM physics in this configuration is well understood. The storage ring option is very promising and will be further studied. The design of the REDTOP detector is largerly independent of the storage ring where it will be installed. Dependent on the timeline of the FAIR construction realization, the REDTOP will either be built at the SIS18 or the ESR of the present GSI or at the SIS100 or the HESR of FAIR.

E. The REDTOP detector for GSI/FAIR

The detector layout proposed for GSI is an optimized version of that used for the Snowmass-2021 sensitivity studies (cfr. Sec. in Sec. III and reference [5]), and derives from a better understanding of the background. The most relevant changes are summarized below:

- The ten Li foils with 10 mm diameter making the target system are replaced by 5 Be foils with 2 mm diameter. The smaller size allows them to be spaced 2.5 cm apart (rather than 10 cm, as for the Snowmass-2021 layout). The length of the target system is considerably shorter: only 7.5 cm, corresponding to a reduction of 92.5%.
- The scintillating fiber option for the vertex detector has been abandoned in favor of silicon pixel technology. The overall dimensions of the vtx detector are, also, much smaller, thanks to the reduced size of the target system.
- A double-layer Čerenkov Threshold Detector replaces the single-layer version;
- The rear section of the (integrally active) ADRIANO2 detector is replaced by a triple-readout, sampling ADRIANO3 version.

The barrel length of the proposed layout is $\sim 33\%$ shorter than the previous version, thanks to the shorter target system, considerably reducing the cost of the experiment. Preliminary studies indicate that the sensitivity improves by approximately a factor of two compared to the Snowmass layout used for the studies presented in Sec. III. Therefore, the effect of a high-resolution vertex detector more than compensates for the smaller production of η/η', due to the reduced target size.

The individual components of the REDTOP detector are briefly discussed below. A sketch of the detector is shown in Fig. 19. The requirements for each subdetector are derived from the sensitivity studies found in reference [5].

1. The target systems

The target system depends necessarily from the beam configuration chosen for the experiment (see Sec. V D above). They are discussed separately for the two options under consideration.

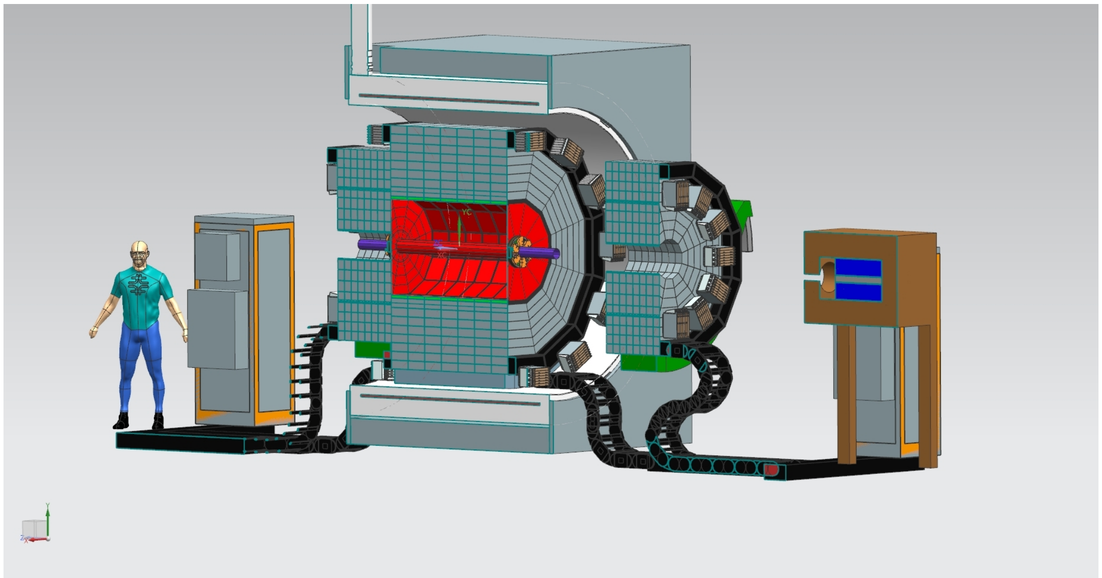

FIG. 19. Cross section of REDTOP detector

Target system for the SIS18 beam option
Two target systems are under consideration for the SIS18 beam option: multiple solid foils of Li or Be and liquid Deuterium (LDe).

The solid foils configuration has been studied extensively for the Snowmass-2021 study program. A lithium target has the advantage of a slightly lower neutron background ($\simeq 2$ neutrons/event vs $\simeq 3$ for beryllium), which has negligible effect on sensitivity to BSM physics. On the other side, lithium is more difficult to handle, and it requires more R&D.

A target made of LDe enclosed in a 5 cm long kapton barrel of 50 μm thickness has been studied in some detail. The interaction rate for a 10^{11} POT/s beam would be $\sim 420MHz$, with $\sim 1\%$ of the scatterings occurring in the kapton window. The main advantage of this target system is that the background is considerably lower. In fact, a study with *GenieHad-Urqmd* indicates that the multiplicity of primary particles generated in the above target at 1.8 GeV for events without an η is about 2.0 for charged (mostly, protons and pions) and 1.4 for neutral particles (to be compared with 3.8 charged and 3.0 neutral in Be). The main disadvantage of a LDe target is in the higher complexity of the system, although similar systems have been built in the past (see, for example, [68] and references therein). Another disadvantage is that the η/η' decay products are subject to a larger multiple scattering when they propagate trough the volume of LDe.

Target system for the storage ring option
As discussed in Sec. V D, the beam lifetime and the required luminosity impose conflicting constraints on the target system of this running configuration. Two target systems are under consideration in such case: a Be wire and gaseous De. With a Be wire, the proton-nucleus interaction probability is mainly controlled by the geometrical cross-section ratio between the beam and the target. A target system consisting of a wire with a diameter of 20 μm,

for example, illuminated by a beam with a radius of 1 cm would have a proton-nucleus interaction probability of $\sim 4 \times 10^{-7}$, which falls within the limits established above. The advantages of this configuration consist in a very simple mechanical implementation of the system and in the very precise knowledge of the primary interaction in the $y - z$ plane.

A gaseous/cluster/pellets De target of appropriate density, as, for example, that designed for the PANDA experiment, would also fulfil the proton-nucleus interaction probability constraint, although the system is considerably more complex and its integration in a hermetic detector like REDTOP could be challenging.

In conclusion, a several target/beam configurations for running at GSI (or FAIR) have been identified. Among them, the solid foil target with an extracted beam has been studied in details and the sensitivity of that running configuration to BSM physics is well understood. Further studies will be carried out to compare the other options before the design of the experiment is finalized.

2. The vertex detector

The vertex detector has four main tasks: a) identifying events with a detached secondary vertex; b) contributing to the reconstruction of charged tracks originating from the target; c) rejecting photons converting in the target; and d) reconstructing tracks with very low transverse momentum. The most critical aspects of REDTOP vertex detector are related to the material budget and to its proximity to the interaction region. Keeping the material budget as low as possible is a necessary requirement to reduce multiple scattering, which, in the momentum range of interest for REDTOP, is the major source of resolution loss. An excessive amount of material would also increase the background from photon conversion. The main requirements for the vertex detector, are listed below:

- A spatial resolution near the IP better than 20 μm;
- Material budget: <0.1% X_0/layer;
- timing resolution of a few ns;
- Radiation hardness up to $\sim 5 \times 10^6/\mathrm{cm}^2/\mathrm{s}$ "*1-MeV equivalent neutron fluence*" or $\sim 5 \times 10^{13}/\mathrm{cm}^2$ integrated over 1 year ;
- Coverage: >90% of full solid angle.

The requirements for the vertex detector are similar to those of the pixel tracker of the Mu3e experiment at PSI (muon stopping rate $\simeq 100 MHz$ in phase-1 and $\simeq 2000 MHz$ in phase-2, vs inelastic event rate $\simeq 500 - 700\ MHz$ for REDTOP, maximum track momentum $\simeq 53\ MeV/c$ vs $\simeq 1.1\ GeV/c$ for pions and $\simeq 2.2\ GeV/c$ for protons in REDTOP). Therefore, we adopted the same HV-MAPS technology as Mu3e, based on the MuPix sensor [69]. It was recently demonstrated that that technology can reach a time resolution of $6 - 8\ ns$ with appropriate time-walk correction [70], which also fits well with REDTOP requirements.

The vertex detector for REDTOP consists of three layers of HV-MAP sensors for the barrel and for the endcaps. The innermost layer is located at a distance of 2.4 cm from the beam axis, while the radius of the outermost layer is $\sim 4.2\ cm$. The total detector length depends on the design of the target system. For the proposed layout, the detector is 28 cm long with a solid angle coverage of $\sim 91\%$. The pixel size is dictated by the deviation that particles with momentum $\mathcal{O}(100\ MeV\ MeV/c)$ undergo between two layers because of multiple scattering. In the case of REDTOP, that size corresponds to $80-100\ \mu m$, which is also similar to Mu3e. Hit timestamps are derived from an internal phase-locked loop (PLL) running at a frequency of 625 MHz. A timing resolution of 6 ns has been obtained with the latest version of the MuPix sensor.[2] A schematic of the layout of REDTOP vertex detector is shown in Fig. 20.

The vertex detector will consume about 0.8 kW of power, corresponding to ∼400 mW/cm^2 [68]. A cooling system based on cold gas at ambient conditions is sufficient to keep the temperature of the detector below 70 ^{o}C (corresponding to the glass-transition temperature of the adhesives used for construction).

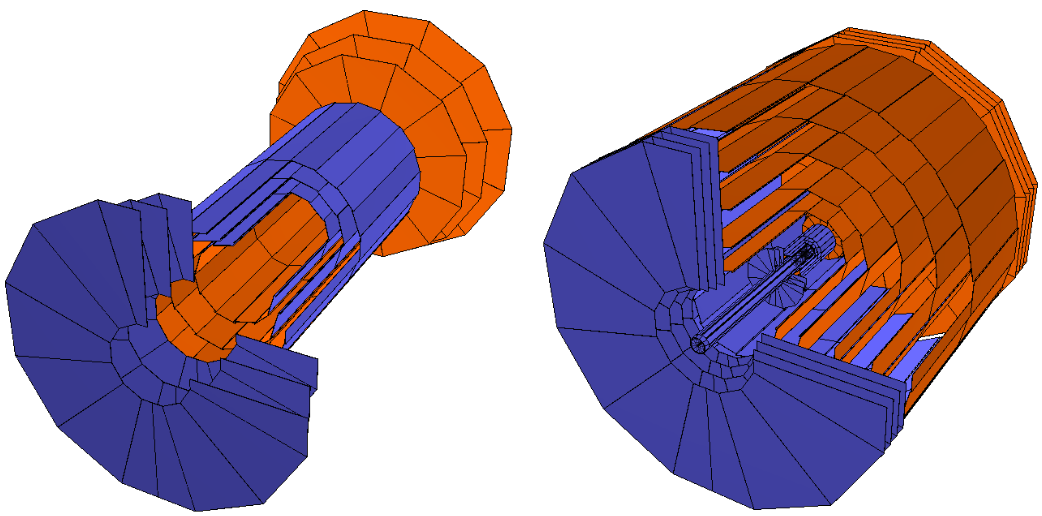

FIG. 20. Schematics of the vertex detector (left) and of the central tracking system of REDTOP (right).

3. The central tracker

A new generation, 4-D tracking system is proposed for REDTOP, to complement the vertex detector in reconstructing charged tracks and the *CTOF* system in disentangling

[2] with offline time-walk corrections [70]

leptons from hadrons. At the same time, the material budget needs to be kept low to reduce multiple scattering for low momentum tracks. The main requirements for the central tracker (cfr. reference [5]) are listed below:

- Momentum resolution: $\sigma_{P_T}/P_T^2 \sim 2 \times 10^{-3}$ GeV^{-1}at P$_T$=1 GeV;
- Material budget: ∼0.1% X_0/layer;
- Time resolutions: < 30 ps/layer;

Current LGAD sensor technology can meet the timing and momentum performance requirements of REDTOP. The ATLAS and CMS collaborations have planned dedicated layers of LGAD detectors for the forward regions to measure the time of arrival of particles, with a primary motivation being the rejection of tracks from pileup events [71, 72]. Radiation hardness is a primary consideration for these detectors, since they must tolerate fluences well over 10^{15} $\mathrm{n_{eq}/cm^2}$. Both detectors plan a spatial granularity of 1.3×1.3 $\mu\mathrm{m}^2$.

The pixel size of the REDTOP central tracker is dictated by the deviation that particles with momentum $\mathcal{O}(100\ MeV\ MeV/c)$ particles undergo between two layers because of multiple scattering. In the case of REDTOP, that size corresponds to $1 - 1.5$ mm, which is close to the pixel size of the CMS ETL.

The majority of the material in the ATLAS and CMS timing layers is cooling and mechanical support, with the sensor and readout chip are typically only comprising a few percent of the total. To meet the material budget of REDTOP, only passive cooling can be used. Carbon-fiber support structures similar to those planned for the HL-LHC upgrade of the pixel detector are strong, lightweight, and have good thermal conductivity. The system, particularly the readout electronics, must be designed to minimize the heat output.

The total thickness of an AC-LGAD layer (base + sensor) can be kept as low as $\simeq 100\mu m$). An estimate of the material budget for the tracking region of the detector which includes the carbon fiber support structure is shown in Fig. 21 as function of the transverse radius. The plots indicate that the beam pipe contributes ≃0.2% of X/X_o, the vertex detector ≃ 0.1% per layer, while the central tracker contribution is ≃ 0.2% per layer.

4. Electromagnetic and hadronic calorimeter: ADRIANO2 and ADRIANO3

Besides measuring the energy and the time of arrival of the impinging particles, the calorimeter system also provides information for the determination of particle ID and to all trigger levels. Therefore, it must provide pre-processed information on a very short time scale. The biggest challenge for the REDTOP calorimeter system is to disentangle the electromagnetic and the hadronic showers, especially those generated by neutral particles

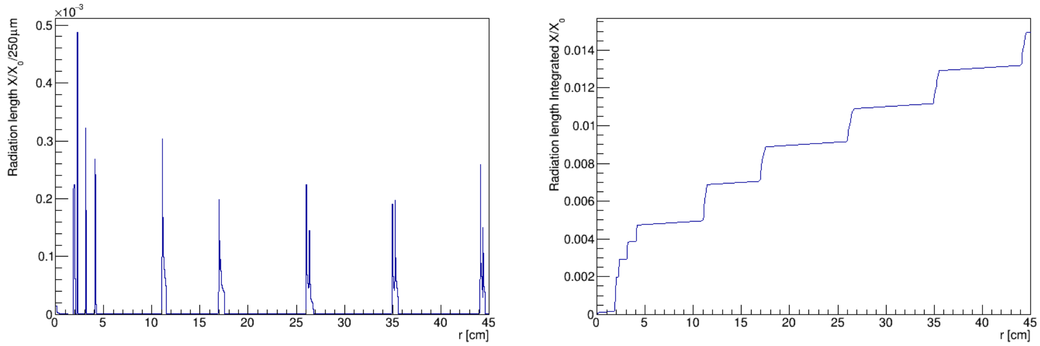

FIG. 21. Plot of X/X_o as a function of the transverse radius for the baseline tracking system of REDTOP. The calculation is performed in radial steps of 250 μm (left). The integrated material budget is shown in the right plot.

(photons and neutrons), as they are not detected by the other systems. A multiple-readout calorimetric technique fulfills all the above needs.

Extensive studies [5] indicate that REDTOP calorimeter systems must have the following requirements:

- Energy resolution: $\sigma_E/E < 2\%/\sqrt{E}$
- High granularity
- Particle Identification (PID) with separation efficiency between electromagnetic and hadronic particles higher than 99% (see also Sec. V);
- Time resolution: < 80 ps in a single cell with energy deposit $>$ 7 photoelectrons;
- Detector response: $<$ 100 ns;
- Reconstruction efficiency: $>$50% for E$>$20 MeV and $>$90% for E$>$80 MeV.

Good energy resolution with high granularity are needed to identify π^0 mesons (mostly decaying into $\gamma\gamma$ and γe^+e^-) produced in the target from the primary interaction or from the decay of the η/η' mesons. The former are responsible for one of the largest combinatoric background.

Particle identification is important to reduce the hadronic background. At the energies of interest for REDTOP, the showers generated by neutrons and photons are almost indistinguishable by pure topological algorithms. Multiple readout-calorimetry, on the other side, has the ability to distinguish electromagnetic vs hadronic vs neutronic showers by comparing the measurements obtained from the individual readouts.

We have estimated that for the BSM's final states with the most energetic photons ($\eta \to \gamma X_{17}$), $\sim$89% of the EM barrel (endcap) showers have 80% of their energy deposited within the first 6.5 (11) X_0's and 90% of their energy deposited within the first 7.8 (17) X_0's. The above considerations has driven the design of the calorimeter which is divided into two sections. The innermost ∼17 cm (28 cm) of the barrel (endcap), corresponding to ∼8 (13) $^X/_{X_0}$, implements a dual-readout technique called $ADRIANO2$ [73, 74]. The latter consists of alternating tiles of SF57 lead-glass and scintillating plastics, optically separated and read-out individually by on-tile SiPM's. For an optimal collection of the Čerenkov light, the lead-glass tiles (size = 1×3×3 cm^3) are coated with either a diffuse ($BaSO_4$) or reflecting metal (for example Ag, Al, Mo, W, etc.) The scintillating tiles have a size = 0.4×3×3 cm^3.

The outermost section of the barrel (endcap) calorimeter, about 53 (67) cm in depth, is based on the new ADRIANO3 triple-readout concept. This consists of alternating layers of $ADRIANO2$ tiles (using 1.5 cm thick ZF2 glass, rather than SF57), a thin glass RPC and 5 mm of a passive absorber (steel). One layer of RPC's is installed every four layers of $ADRIANO2$. The latter increases the nuclear interaction lengths of the calorimeter so that the hadronic showers are better contained within the detector. The overall dept of the two calorimeter sections corresponds to ~ 25 (~ 35) $^X/_{X_0}$ for the barrel (endcap) and ~ 2.8 (~ 4) λ_I.

One of the advantages of dual and triple-readout techniques is that they provide a way to identify a particle by comparing the response of the various calorimeter components. The concept of particle separation with a dual-readout calorimeter is illustrated in Fig. 22 for particles of different species corresponding to the signal ($\eta \to \gamma A'_{17} \to \gamma e^+e^-$) and the QCD background. The separation between photons and neutrons (left plot), is larger than 4σ, and it far exceeds the required value of 99% for the PID of those particles. It is worth nothing that the response of a conventional, single-readout, calorimeter measuring dE/dx corresponds to the projection of the scatter plots on the $y-axis$. In such case, the identification of the particle species would be almost completely lost, especially for photons and neutrons.

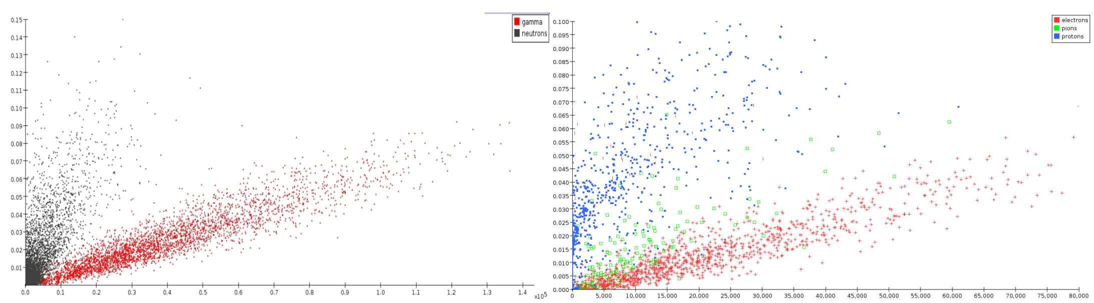

FIG. 22. Plot of the scintillator(S) vs Č signals (a.u.) in ADRIANO2 for neutral (left, photons in red and neutrons in black) and charged particles (right, electrons in red, pions in green, and protons in blue). The EM particles (γ, e^+, e^-) are from the process: $\eta \to \gamma A'_{17} \to \gamma e^+e^-$, while the hadrons correspond to the QCD background generated with GenieHad.

For hadronic showers, the multiple-readout technique also implements the compensation of energy measurements on an event-by-event basis, which reduces the stochastic fluctuations and improves the energy resolution of the detector for hadrons. Thin RPC's with ^{10}B doped glass implement the third readout of ADRIANO3, the rear section of REDTOP calorimeter. The $\alpha - particles$ generated by the reaction ${}^{10}_{5}B +^{1}_{0} n \rightarrow\ {}^{7}_{3}Li +^{4}_{2} He$ will be detected by the RPC gas with great efficiency. The corresponding readout will be the third independent readout largely sensitive to neutrons. Studies are in progress to optimize the layout of ADRIANO3 and to estimate the sensitivity of such device to neutrons with energy of several hundred MeV.

The high granularity of the calorimeter imposes certain challenging specifications for the front-end and readout electronics. The main requirements are: high dynamic range, low noise, and high-precision time information. Since the readout will be embedded in the detector built mostly of lead-glass, the power consumption should not exceed $\sim$ 25 mW/ch. Finally, information from the scintillation and Čerenkov components are sent to the Level-0 trigger, which requires a low-latency architecture.

High-performance ASIC's (HGCROC3, and TOFHIR2) are under development for HL-CMS upgrades with adequate timing resolution (25 - 40 ps) and power consumption (20 mW/ch). Both chips can be easily adapted to the lower light yield from ADRIANO by fine-tuning the gain of the internal pre-amplifier. The main challenge for the adoption of the HGCROC3, which is being considered for ADRIANO2(3), consists in the fact that it is designed to readout the entire calorimeter data at LHC beam crossing rate (40 MHz), about one order of magnitude slower than REDTOP's inelastic event rate. On the other side, the event topology at an η/η'-factory is substantially different than at LHC. More specifically, the average event multiplicity at REDTOP is only $\sim$ 7 particles, vs $\sim 10^4$ for LHC-HL, with an average detector occupancy of $\sim 3.5 \times 10^{-4}$. To accommodate the different topology, the readout system for the detector will be divided into "region of interests" (ROI) and only those which have data will be readout. Thanks to the low event multiplicity, the readout of the ROI's will occur at a much lower rate, matching the 40 MHz readout limit of the HCGROC3 chip. Studies are in progress to optimize the readout strategy.

5. *The Threshold Čerenkov Time of Flight (CTOF)*

A thin Čerenkov radiator, with relatively low refractive index, is inserted between the central tracker and the calorimeter. The detector has two main purposes: a) the detection of particles above the Čerenkov threshold and b) the measurement of the TOF of such particles. The information from the $CTOF$ is also used in the Level-0 trigger to reduce the contamination of the signal events from the very abundant, but slow baryonic particles. Finally, the $CTOF$ complements the energy measurements of the calorimeter as it operates as a lower density pre-shower.

The requirements for the $CTOF$ are:

- $n_D < 1.45$, which makes it blind to protons with E_{kin}<400 MeV;

- Time resolutions: $< 50\ ps$;
- Detector response: within $100\ ns$
- High-granularity to reduce pile-up.

The baseline layout of the $CTOF$ consists of two layers of small quartz tiles. The momentum threshold for the various particle species is summarized in Table X. The tiles have the the

TABLE X. Čerenkov threshold of $CTOF$ detector.

PID	***Momentum threshold [MeV/c]***
electron	0.4
muon	100
pion	130
proton	870

same footprint of ADRIANO2 tiles (i.e., $3 \times 3 \times 1\ cm^3$). The Čerenkov light is read-out by four, actively ganged, NUV-SiPM's, which are optically coupled to each unit. The SiPMs are soldered to a printed circuit board (PCB), which is connected via a flexible PCB (flexprint) to one of the ASIC on the readout board. An intrinsic time resolution of ≃50 ps for the individual tiles has been measured by T1604 Collaboration at a recent test beam. A radiator consisting of two layers, as proposed for REDTOP, will exceed the time resolution requirement for the $CTOF$.

The resolution and readout requirements for the $CTOF$ are similar to those established for the MTD Endcap Timing Layer of the CMS experiment (50 ps per hit and 35 ps per track, with data readout based on a 320 MHz clock). Therefore, the same readout electronics and architecture, based on the ETROC2 could be used with minor modifications for REDTOP's $CTOF$. The main difference between the two detectors is in the charge generated by the different sensor technologies employed (SiPM vs LGAD), which can easily be compensated with an appropriate charge conveyor between the SiPM and the ASIC.

6. The Timing Layer (TL, optional)

Further improvement to the PID systems could come from the TOF system when the requirement on timing resolution of the $CTOF$ is lowered to 30 psec or less. Preliminary studies performed by T1604 collaboration indicate that such a resolution could be beyond the limits of the technology adopted by the $CTOF$. An optional AC-LGAD Timing Layer (TL), based on the design planned for experiments at the Electron Ion Collider (EIC), would be able to reach the desired goal. The proposed layout for REDTOP would employ the $CTOF$ as supporting structure, contributing to a small fraction of the material budget of the TL, with negligible impact on the performance of the ADRIANO2 calorimeter.

7. *Superconducting solenoid*

A 0.6 T solenoidal magnetic field is required to measure the P_t of the particles with $\beta \approx 1$. The field will also magnetically bottle the very low momentum particles, preventing them from reaching the calorimeter. The solenoid built for the, now dismantled, Finuda experiments [**?**] matches all operational and dimensional parameter required for REDTOP. It also fits the space available for both experimental areas options considered for the experiment at GSI.[3].

F. The event trigger systems

The goal of producing 5.2×10^{13} η mesons per year, (5.2×10^{6} η/s, assuming 10^7 seconds of useful running time), requires about 7×10^8 p-target inelastic collisions per second. (cf. Table IX). This rate can be achieved with a proton beam intensity of 10^{11} p/s and a Li or Be target of 2×10^{-2} collision lengths ($\approx$ 7.7 or 2.3 mm total thickness), possibly subdivided into a number of thinner layers. Taking into account the total p-Li (or p-Be) inelastic collision rate, we estimate that the total rate of events reaching the detector is $\sim 7 \times 10^8$ Hz. The vast majority of particles entering the REDTOP detector are hadrons produced by inelastic scattering of the proton beam on nuclear matter. The average multiplicity p-Li (p-Be) interaction is found to be 3.5 (3.8) for the charged and 1.8 (1.9) for the neutral hadrons.

The event rate is more than one order of magnitude larger than the event rate observed in the LHCb experiment [75], indicating that either very fast detector technologies and/or topological trigger strategies need to be implemented along with a multi-level trigger systems, finely tuned for the expected event structure. We envisage a three level (L0, L1, L2) trigger to successfully reduce rates to acceptable levels. Risk will be significantly reduced by adopting technology and techniques developed for other experiments. System performance is summarized below after introducing the three trigger levels.

1. *Level-0 trigger*

The selection performed at the Level-0 trigger is based on simple global features of the events produced by p-target inelastic collisions. All events interesting for NP have at least either two leptons or two pions in their final state, often in association with at least one energetic photon in the calorimeter. The purpose of the Level-0 trigger is rejecting non-interesting events with a time lag of few tens of nanoseconds. The leptons and pions originating from the decay of the η meson are more energetic than those generated by the proton-nucleus interaction, and usually their velocity is above the $CTOF$ threshold. The

[3] The solenoid will be operated at $\sim 1/2$ the field intensity, requiring much less iron for the return yoke

corresponding TOF is, also, smaller. Therefore, the fast signals produced by the $CTOF$ and by the ADRIANO2/3 sub-detectors are the primary input to the Level-0 trigger system.

The strategy implemented in the Level-0 trigger is the following:

- a minimum Čerenkov energy from ADRIANO2 integrated over the whole detector;
- at least two clusters in the CTOF with energy above threshold and TOF below a defined value;
- the integrated scintillation/Čerenkov signals ratio from ADRIANO2 must be compatible with an electromagnetic shower.

The data rate into Level-0 is estimated with Monte Carlo simulations. The reduction factor of the event rate is ~ 4.6 and the average event size is $\sim$1.5 kb, after zero suppression and compression by the DAC. Assuming a 12-bit digitization for charge and time and an 18-bit address to identify the struck cells at a maximum collision rate of 700 MHz, we conclude that the average rate of the data sent to the Level-1 trigger does not exceed $\sim$230 Gb/s. Such a data rate can be comfortably transmitted by a network of a few hundred optical fiber links. Because all data from the detector are continuously digitized in the front-end and immediately transmitted to the following stages, trigger latency is not expected to be a problem, at least to first order. Therefore the Level-0 logic can be heavily pipelined. Although a new event will arrive, on average, every 1.4 ns, the time taken to make a decision on a specific event can be much longer, possibly of the order of hundreds of nanoseconds.

2. Level-1 trigger

In contrast with the global aspects of Level-0 input, the Level-1 rejection is based on local information obtained directly from the sub-detectors. That requires the implementation of at least low-level pattern recognition and clusterization of the hits. Considering the low level of occupancy in the tracking system, the Level-1 trigger can be easily implemented by Vertically Integrated Pattern Recognition Associative Memory(VIPRAM) [76]. The trigger strategy for the present studies are intended to reduce the background from baryons as well as from photons converting into an e^+e^- pair in the innermost region of the detector.

The set of requirements for the Level-1 trigger is listed below, grouped by the specific type of background targeted:

Baryon rejection

- at least three clusters in the LGAD tracker, separated by a distance of 4.5 mm or larger;
- at least two groups of hits with three LGAD clusters and one $CTOF$ cluster, consistent with oppositely charged particles, and with TOF below a defined threshold;

- the integrated energy in the $CTOF$ for positive and negative tracks has to exceed a defined threshold;
- at least three ADRIANO2 clusters with scintillation/Čerenkov ratio consistent with a non-baryonic particle.

$\gamma \to e^+e^-$ rejection

- No clusters in the vertex detector, associated to two oppositely charged tracks, separated by less than 3 mm in the $r - \phi$ plane and in the z-direction;
- No clusters in the Central Tracker associated to two oppositely charged tracks separated by a distance shorter than of 4.5 mm.

The acceptance of the Level-1 trigger for p-Li inelastic collisions (background), and for several topologies of signal events, is shown in Table XI. Factorizing the event reduction (cfr. reference [5]), the data sent from the Level-1 trigger to the Level-2 trigger is about 3.8 Gb/s. Such a data rate can be comfortably transmitted by a network of a few hundred optical fiber links.

A significant challenge of the REDTOP trigger will be to design specialized processors to achieve the needed rejection factor of under 2% by reconstructing proto-tracks with high efficiency, at an event rate of 100 kHz. We believe that this selectivity can only be achieved with specialized hardware, possibly based on massive use of FPGAs. To gain more time to process each event, we can adopt a time multiplexing strategy. We anticipate that events will be distributed to a bank of identical processors in a round-robin fashion. The larger the number of processors, the more time each one of them will have to process one event. A time multiplexing of a factor of 10 will allow each processor 5 microseconds, on average, to process each event, which seems adequate for the task.

3. Level-2 trigger

The Level-2 trigger aims to positively identify the underlying physics process and, therefore, it relies heavily on the topology of the final state. The algorithm implemented requires a fully reconstructed event, including: a) the identification of the target foil where the primary interaction occurred, b) the approximate reconstruction of tracks and calorimetric showers, c) identification of potential secondary vertices.

The requirement on the final state topology for discriminating the event at the Level-2 trigger are:

- at least two fully identified leptons;
- two oppositely charged pions and two calorimetric showers;

- four pions;
- any two oppositely charged tracks with a secondary vertex detached by more than 5 cm from the primary interaction.

The acceptance of the Level-2 trigger for p-Li inelastic collisions (background), and several topologies of signal events is shown in Table XI.

The Level-2 will be implemented entirely in software. The processor farm will receive 2.5 MHz of events, equivalent to a data rate of ∼3.8 GB/s, from Level 1. These events need to be reconstructed, filtered and formatted for permanent storage. We assume that this task can be completed by using less than 100 ms of CPU time and that, consequently, a farm of 2000 CPUs should be adequate for the job.

4. Digitization and Compression: Summary of Trigger Performance

The task of the REDTOP trigger systems is to reduce the event rate from the total inelastic collision rate of$\sim 7 \times 10^8$ Hz down to about 3 MHz of events to be permanently recorded. Assuming a 12-bit digitization for charge and time and an 18-bit address to identify the struck cell, we conclude that the average size of the final event surviving all levels of trigger is about 1.6×10^3 bytes. A summary of the expected data throughput is presented in Table XI. Such yield will produce an output data rate of ∼0.9 Gb/s or about∼ 9 PB/year, which we consider manageable.

The needed $\sim 2.3 \times 10^3$ reduction in event rate is achieved by three trigger stages. These three stages are preceded by a digitization and compression (DAC) stage. The DAC stage is directly connected to the front-end of the detector. Level-0 and Level-1 are located off the detector. A fiber optics network delivers data from the DAC to Level-0 and from Level-0 to Level-1. The events filtered by Level-1 are delivered to Level-2, a processor farm that performs event building, reconstruction, formatting, and classification. A further rate reduction can possibly be achieved at Level-2, before permanent recording, if needed. Table XI summarizes data and event rates into and out of the different stages.

TABLE XI. Data and event rates for different stages.

Trigger stage	*Input event rate Hz*	*Event size bytes*	*Input data rate bytes/s*	*Event rejection*
Level 0	$7. \times 10^8$	1.4×10^3	9.8×10^{11}	∼4.6
Level 1	1.5×10^8	1.5×10^3	2.3×10^{11}	∼60
Level 2	2.5×10^6	1.5×10^3	3.8×10^9	∼4.5
Storage	0.56×10^6	1.6×10^3	0.9×10^9	

Future improvements in the detector design are expected to reduce the background further. In particular, we foresee the adoption of a topological trigger strategy, rather than a global one which was implemented in the present studies. The former is expected to improve considerably the rejection factor of the Level-0 trigger.

G. Computing

The REDTOP computing model is discussed at great detail in ref. [77]. Based on the computing resources currently utilized on the Open Science Grid (OSG) for the sensitivities studies, we estimate that the reconstruction of the raw data and the Montecarlo simulations will amount to $\simeq 40M\ cpu - hours/month$. We expect that about 80% of that computing will be from an opportunistic use of the OSGPool (namely, at no cost). The remaining 20% will be from dedicated cpu's located at REDTOP participating institutions, federated with the national OSPool. Approximately $3/4$ (or $\simeq 12,000$) of the dedicated cpu's are already existing at the Computing Centers of such institutions. The remaining (or $\simeq 3,000$) will be purchased, if necessary at the time when the experiment will run, as part of the project costs. The resulting annual data volume of about 9 PB/yr can be accommodated already by the existing infrastructure of disk and tape arrays at GSI.

When not in use, the 2,000 CPU dedicated to the Level-2 trigger (plus the spare 560 cpu's from the EPIC) can be used to partially fulfill that task. Then the data will be transferred to the central GSI computing center, where it is stored and analyzed.

VI. DETECTOR R&D

Almost all REDTOP sub-detectors rely on state-of-the-art technologies which are already under development for new experiments or upgrades of existing experiments. The only exceptions are the electromagnetic and hadronic calorimeters, as multiple-readout calorimetry has never been implemented before in a real experiment. Consequently, only minor R&D is required for the tracking detectors and for the $CTOF$, mostly aiming at optimizing the technologies and the design for REDTOP. The amount of R&D depends on the detector component. It has been estimated in about two years for each sub-detector and three years for the trigger systems. The estimated effort is reflected in the chart in Fig. 23 for the project timeline.

A detailed discussion of the status of the R&D for each sub-component of REDTOP is presented in Appendix II.

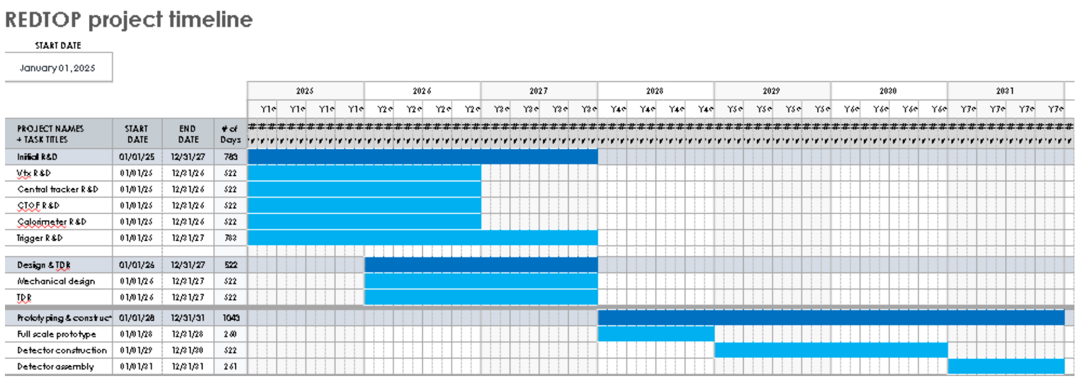

FIG. 23. REDTOP R&D and construction timeline

VII. TIMELINE, RESPONSIBILITIES AND COSTS

A. Timeline

Many of the detector technologies adopted for REDTOP require modest R&D effort (as described in the detector R&D appendix). Also, considerable effort is required for the technical design of the experiment. In any case, for both efforts, project funding must be in place. Therefore, the starting date of the REDTOP initiative can be identified once all Detector R&D and engineering design funds are established for the institutions involved in the relevant activities.

Under the assumption that the starting date of the project is 1/1/2025, a preliminary timeline for the various stages of the experiment is presented in Fig. 23 for the R&D and construction phases. Note, that, except for the trigger, detector R&D will be completed in two years and engineering and technical design will be completed in three years. Detector prototyping, construction and assembly will occur over a four-year period. A year will be required for commissioning the experiment, during which we will ask GSI for short periods of beam at increasing intensity. The length of the physics runs depends on the availability of the beam, and it is discussed in more detail in Sec. VIII.

In conclusion, the entire project will require a bit more than a decade for realization and exploitation. Assuming subsequent upgrades, the REDTOP program will provide a decades-long physics program.

B. Institutional Responsibilities

The REDTOP collaboration is already quite strong with over 50 collaborating institutions. All of these institutions have strong interests and excellent capability for specific aspects of the detector including the beamline, magnet, vertex detector, central tracker, time-of-flight detector, and calorimeter. There are ample opportunities for further collaborators especially in the trigger and DAQ systems, which because of their vertical nature, are excellent laboratory projects. Details are provided below.

1. Beamline

Once the decision on the realisation of REDTOP experiment at GSI/FAIR is taken, the GSI/FAIR will be the host laboratories and fulfil the hostlab duties. This includes the assistance from various GSI/FAIR technical groups, like vacuum, construction, assembly, power supplies, magnets, safety, etc. Once precisely specified, a dedicated request to GSI/FAIR laboratories will be submitted.

2. Target

The cutting of beryllium foils cn be performed by commercial companies which have served GSI for a long time. The final assembly of foils and of the beam pipe can be performed in the Target Laboratory of GSI.

3. Magnet

The dismantling and transportation of FINUDA Magnet require the involvement of the Engineering Depts. of the two Laboratories (GSI and INFN-LNF). This task will mainly be coordinated by the GSI and the experiment management.

4. Vertex detector

The technology for the silicon vertex detector has been chosen only very recently, between the two options under consideration. The vertex detector is based on the MuPix sensor technology which has been developed for the Mu3e experiment by the Karlsruhe Institut fur technology (KIT, Karlsruhe, Germany). The group at Argonne National Laboratory (Illinois, USA) has expressed interest in taking the responsibility for the design and construction of this detector. The responsibility includes also the integration of the front-end readout system with the DAQ of the experiment.

5. Central tracker

The silicon central tracker is based on the AC-LGAD technology which has been developed for the CMS-Upgrade experiment by the Centro Nacional de Microelectronica

(CNM, Barcelona, Spain). The group at University of Illinois Chicago (USA) has expressed interest in taking responsibility for the design and construction of the multi-layer silicon detector. The responsibility also includes the integration of the front-end readout system with the DAQ of the experiment.

6. Čerenkov Time of Flight

The Čerenkov time-of-flight detector is based on technology (JGS1 tiles with SiPM-on-tile readout) under development by the T1604 Collaboration. Tsinghua University, (also a member of T1604) is interested in taking responsibility for the construction of this component. The readout, based on the ETL or the TOFHIR2 chip, will be developed separately. The proponents are currently searching for interested parties and groups willing to take responsibility for the readout systems.

7. Calorimeter

The ADRIANO2 (EM) and ADRIANO3 (hadronic) calorimeters are presently under development by the the T1604 and the ADRIANO3 Collaborations. Fairfield University, Northern Illinois University, University of Iowa, and Beykent University (members of the above collaborations) have expressed interest in designing and building the calorimeter systems of REDTOP. The responsibility also includes the development of the front-end readout system and its integration with the DAQ of the experiment.

8. Trigger

The proponents are currently searching for interested parties and groups willing to take responsibility for the trigger systems of the experiment.

9. Data Acquisition and Slow Control

The proponents are currently searching for interested parties and groups willing to take responsibility for the Data Acquisition and Slow Control systems of the experiment.

10. Data Analysis and Simulation

It is expected that all participating groups are contributing to the data analysis and simulations.

TABLE XII. REDTOP cost estimate.

Component	M$ [Y2023]
Target+beam pipe	0.1
Vertex detector	2.1
LGAD tracker	22.5
Calorimeter	22.5
CTOF	0.75
Solenoid	0.3
Supporting structure	1.3
Hardware trigger	2.4
DAQ+L2 trigger	1.1
Computing	0.4
Contingency 50% (as per DOE recommendations)	26.7
Total REDTOP	**80.2**

C. Cost estimates

1. *Design and construction*

The optimization of the detector design is proceeding at a steady pace, taking advantage of the fact that a nearly-full simulation and reconstruction framework is in place. Consequently, only an approximate cost estimate is availalbe at this stage of the project. Costing of electronic components and sensors (SiPMs, ASICs, LGADs, etc.) is based on current (i.e., 2023) quotes from vendors. Several components of REDTOP adopt the same technology and design of existing detectors (or their upgrades), for which detailed costing is available. In such cases, the costing for REDTOP is estimated by simply scaling those figures (including inflation) in an appropriate way. Contingency is included in the estimate, but labor is not. The cost estimate for the individual components of the experiment is discussed in detail in Appendix I. The total cost of REDTOP is summarized in Table XII. Details can be found in the cost appendix.

2. *Operating costs*

We assume that the costs for operating the detector and the accelerator and of delivering the beam to the experiment are entirely covered by the hosting laboratory. Other operating costs for the experiment consist mainly in the permanent storage of the offline data at GSI, which will be covered by the experiment. The estimate for the 9 PB/year required by REDTOP is $\sim$0.2 MEu/year.

3. Cost reduction

As part of the optimization process of the detector, the collaboration is exploring solutions to reduce the overall costs of the experiment. At this stage, there are strong opportunities for value engineering of all systems. The largest contributions to the costs of REDTOP (cfr. Table XIII) are related to the calorimeter, due to the large number of readout channels. Studies are in progress aiming at reducing the granularity of ADRIANO2(3) without compromising the physics performance.

VIII. BEAM REQUEST AND EXPERIMENT SENSITIVITY TO BSM PHYSICS

The sensitivity of REDTOP to branching ratios for NP processes has been estimated to be in the range $[10^{-11} - 10^{-8}]$, depending on the process being considered, for an integrated luminosity of $\mathcal{L} \simeq 3.3 \times 10^{18}$ POT (cfr. Sec. III) with the detector layout presented in reference [5]. The maximum instantaneous luminosity sustainable by the detector[4] is $\simeq 1 \times 10^{11}$ POT/s.

We propose GSI provide an integrated luminosity corresponding to $\sim 3 \times 10^{18}$ POT at 1.8 GeV and $\sim 2 \times 10^{18}$ POT at 4 GeV, corresponding to ~ 11 months of data taking for the η run and 8 months for the η' run, at a instantaneous luminosity of $\sim 1 \times 10^{11}$ POT/s. The $\eta(\eta')$ sample produced would be $\sim 2 \times 10^{14}$ ($\sim 1 \times 10^{12}$).

The proposed integrated luminosity will support a rich BSM search program. A study conducted on the $p + Be \to \eta + X$ $with$ $\eta \to \gamma A'$ and $A' \to e^+e^-$ production and decay chain indicates that the sensitivity with the detector proposed for GSI could improve by a factor of $\sim \sqrt{2}$. The sensitivity is proportional to $S/\sqrt{B}$ and it scales as $\sqrt{\mathcal{L}}$. Therefore, we could take advantage of the better performance of the proposed detector by running with smaller integrated luminosities. Several models of physics BSM predicts branching ratios smaller than $\sim 10^{-9}$ requiring a sample of reconstructed η mesons of at least order of $\mathcal{O}(10^{11})$. Although the full requested luminosity will permit REDTOP to search for a broad range of new physic, the physics program will begin immediately; when the reconstruction efficiency is factored in, we consider an integrated luminosity corresponding to 10% of that requested above sufficiently sensitive for probing servaer channels for BSM physics with rare η/η' decays.

[4] Here we assume that no pile-up of events occurs in the detector. In a condition where pile-up can be resolved in the reconstruction phase of the offline, a larger instantaneous luminosity could be tolerated.

APPENDIX I: DETAILS OF COST ESTIMATE

The following sections provide some details on the cost estimation method for the various components of the experiment.

1. *Solenoid*

The Collaboration intends to re-use the Finuda magnet[78], currently stored at the *Laboratori Nazionali di Frascati* of INFN. A cost of about \$ 0.3M has been estimated for refurbishing the Dewar vessel, dismantling and shipping the cryostat and the return yoke. Cryogenics (cooler+power supply) is expected to be available at the hosting laboratory.

2. *Supporting structure*

The entire detector will be enclosed in a 1 cm thick, cylindrical steel supporting vessel, held inside the solenoid by two longitudinal rails. The cost of the vessel and the fixtures, including engineering, has been estimated at about \$ 1.3M.

3. *Target systems and beam pipe*

Beryllium foils with a sub-mm thickness are commercially available at modest cost (∼ \$ 1k) [79]. Laser-cutting the foil to the correct shape and size is also handled by commercial firms already serving GSI. Installing the foils inside the beam pipe can be handled by GSI Target Laboratory. The total estimated cost for engineering, components and manufacturing has been conservatively assessed to be no more than \$0.1M

4. *Vertex detector*

The cost of REDTOP vertex detector is derived from the Mu3e pixel tracker by scaling the sensitive surfaces of the two experiments, since sensors, readout electronics and the mechanical structures are the same. Assuming that an existing sensors can be used, the estimate costs of that component is about \$120 per cm^2 active area [80]. This value includes several readout-flexes, HV, LV and data-cables, connectors, and HV and LV supplies and interfaces PCBs. We note that this value is smaller compared to ATLAS ITK pixel, mainly due to savings of the interconnects. Scaling this price to REDTOP's vertex detector area results in a cost of about \$250k, which we double to take into account eventual R&D. We conservatively assume that dedicated sensors need to be developed for REDTOP. This is because the Mupix11 sensors used by Mu3e have a continuous readout and no trigger buffers.

If a triggered readout is required, a new sensor needs to be produced. Each Engineering Run costs about \$200k, which we are conservatively including in the current cost estimate (two runs). In Mu3e a new and innovative gaseous helium cooling system is used which can deliver 50g/s at -20^{o}C. Preliminary engineering considerations indicate that a flux of 10g/s would be sufficient for REDTOP, considering the smaller area which needs to be cooled down. Based on the Mu3e experience, the cooling system for REDTOP willl cost about \$400k, including the chiller, heat exchangers, turbo pumps and pipes.

In summary, we estimate a cost of about \$2.1M for the design and construction of the vertex detector.

5. Central tracker

The LGAD tracker is based on the technology under development for the Endcap Timing Layer (ETL) of the CMS experiment. The sensor, readout chip, and powering cost is based on a recent (2022) report on that project to the CMS institutional board, scaled by the ratio of the surface areas (9.4/7.9). Carbon fiber (thermal pyrolitic graphite) is proposed for the mechanical structure due to its thermal transport properties, stiffness, and low contribution to the material budget. The cost estimate for it is based on the costs for the CMS pixel endcap upgrade for the HL-LHC and scaled to the area of this detector. The layout and dimensions in the case of REDTOP is such that an active cooling can be replaced by passive cooling.

6. ADRIANO2(3)

The granularity of ADRIANO2(3) calorimeter is very similar to that of the HGCAL of CMS and readout electronics are the same. The costing of the latter is, therefore, used as a template for REDTOP. The mechanical structure of the calorimeter is scaled by the total volume of the two subdetectors (8.6 m^3 vs 14 m^3). The water cooling adopted by REDTOP is substantially cheaper than the dual-phase system designed for CMS's HGCAL. Its cost is estimated separately. The cost of the scintillating tiles, the readout, power and slow control systems are obtained by scaling CMS HGCAL by the total number of readout channels ($1.15\text{x}10^6$ vs $6.24\text{x}10^6$)[81, 82]. The SiPM's for REDTOP are provided by a different vendor (Broadcom rather than Hamamatsu) and are costed based on an actual quote from the vendor.

The cost per m^2 for the thin-RPC system is obtained from the large-scale CALICE Digital Hadron Calorimeter (DHCAL) prototype [83]. The estimate (corrected for the inflation) includes also the readout and the slow control systems.

*7. Čerenkov TOF (*CTOF*)*

The cost of the *CTOF* has been scaled from the BTL system of the CMS upgrade. The tile material adopted by REDTOP is less expensive than CMS' BGO, and has been costed separately. The cost of the mechanics is scaled based on the surface of the detector (~ 2.9 m^2 vs ~ 38 m^2), while the readout electronics, power and, services are scaled by the number of readout channels ($\sim$ 13,600 vs $\sim$ 331,776).

8. Hardware Trigger

The L0 and L1 of the trigger systems are implemented completely in hardware and receive input from the almost 14K-channel calorimeter and 51K-channel tracker back-end electronics board. The cost estimate for REDTOP trigger system is still in progress. We conservatively assume a cost of $2.4M for this subsystem.

9. DAQ and L2 trigger

The DAQ and the L2 trigger systems consist almost entirely of computing equipment, purchased when needed. The same strategy is used by CMS's Phase-II upgrade. Therefore, the cost estimate for REDTOP DAQ system is obtained by scaling the data throughput of the two experiments (0.9 GB/s vs 61 GB/sec). The value obtained is inflated by 30% to compensate for non directly scalable components.

The cost of the L2 trigger is consistent with an independent estimate for the 2000 CPU receiving data from the L1 trigger. Since network requirements are not stringent, a 10G machine is sufficient. A conservative estimate for 20, dual socket 32 core EPIC AMD with "*hyperthreading*", equipped with 128 processors, each with 2 GB of memory and an SSD, stands at about $ 0.4M. These have 28% more computing power than needed, which can be used as backup or for the reconstruction /analysis of the data. An additional $ 0.4M would cover the cost of networking/infrastructures, for a total of $ 0.8M.

10. Offline computing

Reconstruction of the raw data and Montecarlo simulation require $\sim 60,000$ CPU's. Approximately 80% of them will be accessed in oppurtunistic mode (i.e., at no cost) from the OSPool. The remaining will reside at the collaborating institutions. We conservatively assume that about 3/4 of them (namely, $\sim 9,000$) already exists as part of the computing centers of the collaborating institutions. Only $\sim 3,000$ would need to be purchased. The estimated cost is of order of $400,000.

TABLE XIII. Preliminary cost estimate for target and tracking detectors.

Target+beam pipe	**0.1**
Vertex detector	2.1
Pixel CMOS sensors + test	0.5
Sensor design	0.4
DAQ	0.4
Slow control	0.2
Mechanics	0.2
Cooling	0.4
Central tracker	**22.5**
Mechanics & assembly	6.4
Sensor modules	7.4
Power systems	1.9
Front-end electronics	5.6
Cooling	0.2

11. Contingency

A contingency factor of 50% is included in the present cost estimate because of the early design stage of the subsystems.

12. Summary of costs

Table XIII provides details on the subsystems discussed above. The total expected cost, including contingency, is about \$ 80.2M.

TABLE XIV. Preliminary cost estimate for calorimeter and TOF sysyems.

Calorimeter	**22.5**
Detector	
SF57 tiles	3.0
ZF2 tiles	1.0
Scint. Tiles	1.1
Sipm glass	4.4
Sipm scint.	1.8
RPC	1.5
Mechanics	
Mechanical structures	1.1
Cooling	0.3
Tooling+coating	0.6
Steel plates	0.04
Electronics	
Slow control	0.3
Electronics and electrical systems	5.8
Backend systems (trigger and DAQ)	1.6
CTOF	0.75
Tiles	0.1
Sipm and sensor modules	0.1
Mechanical structures	0.05
FEE	0.11
Power system	0.05
Cooling	0.07
Back-end electronics	0.1
Safety system	0.07
Installation and test infrastructure	0.1

TABLE XV. Preliminary cost estimate for remaing components.

Solenoid	**0.3**
Fabrication	-
Refurbishing, shipping	0.3
Supporting structure	**1.3**
Hardware Trigger	**2.4**
L0 + L1	2.4
DAQ+L2 trigger	**1.1**
DAQ	0.3
L2 trigger	0.8
Offline computing	**0.4**
Computing	0.4
Contingency	**26.7**
Total before contingency	53.5
50% Contingency (as per DOE recommendations)	26.7
Total REDTOP	80.2

APPENDIX II: DETAILS OF DETECTOR R&D

A detailed discussion of the status of the R&D for each sub-component is presented in this appendix, along with an estimate of the effort still required.

A. Target

The beryllium target systems requires thin foils commercially available from several vendors at relatively low cost. The cutting is also performed by specialty companies which have been identified. Therefore, for this target option, minimal R&D is required. More complex options (lithium foils, gaseous or liquid deuterium) require substantial R&D which can be carried over in parallel with the R&D on the detector.

B. Vertex detector

As discussed above, the vertex detector will re-use the same sensors developed for the the pixel tracker of the Mu3e phase-1 experiment, whose requirements are very similar to REDTOP [68]. Some R&D will be needed to cope with the timing resolution of 6 ns of the latest MuPix sensor in an environment where the average interaction rate is $\simeq 500{-}700MHz$ and with a different detector layout. Given the low average charged particle multiplicity ($\simeq 3.8$) and the small size of the MuPix pixel, we anticipate that any event pileup deriving from the inadequate speed of the readout can be resolved during the event reconstruction phase. Effort required for the above R&D is modest and, we are confident that it could be completed in less than two years.

C. Central tracker

The central tracker will benefit from R&D done for the timing layers for the CMS and ATLAS HL-LHC upgrades. The needed timing performance of 30 ps/layer is essentially already achieved. Meeting the material budget will require either no active cooling or active cooling physically displaced from the detectors, which must be verified. This requires understanding the power consumption of both the sensors and ROCs, as well as the thermal design and materials for the support structure. For the latter, we will benefit from the extensive work done for the carbon-fiber support structure of the CMS pixel upgrade as well as industry experience. Another key question is whether the ETROC would work "out of the box" for the central tracker or significant adaptations need to be made to reduce the power consumption and/or expected event rates for REDTOP.

D. *CTOF*

The core technology for the *CTOF* is currently under development by the T1604 Collaboration and by the group at Tsinghua University. The desired timing resolution has been achieved with a Waveform TDC (Sampic) and all key components have been identified. The R&D foreseen for the *CTOF* is mostly related to the mechanical structure and to the adaptation of the ETROC-based readout electronics designed for CMS Endcap Timing layer. The timing requirements of the latter are more stringent than for REDTOP. Detectors with a layout similar to the *CTOF* have been built for various experiments in the past (for example, the tile detector of Mu3e). Given the relatively small size and weight of the device, we do not expect major challenges regarding the mechanics. Some effort is, however, expected to master the connections between the flexprint, the SiPM's, and the ASICs on the readout board. The ETROC is currently designed to operate at 325 MHz, which is very close to the event rate foreseen at REDTOP. Simple tests would be needed to confirm if the speed of the chip can be pushed further or if the ASIC needs to be slightly modified. In summary, we estimated that the required R&D is modest and it can be completed in less than two years.

E. Calorimeters

Extensive R&D has been conducted on dual-readout calorimetry for the past 9 years by the T1015 and T1604 Collaborations at Fermilab. All aspects of the Čerenkov section of ADRIANO2 have been exploited with the construction of multiple prototypes and the realization of several test beams. The scintillation component uses very similar tiles as the HGCAL of CMS, therefore, it requires no further R&D. The thin RPCs used in the triple ADRIANO3 have undergone extensive R&D by Beykent University and University of Iowa groups, as part of the CALICE [84] research program. The largest ADRIANO2 prototype (Čerenkov section only) built so far consists of 63 tiles with seven layers. A twelve layer version with 192 cell pairs is currently under construction, and is expected to be tested with beams in mid-2024.

Two aspects of ADRIANO2(3) still require further studies: a) the number of SiPMs per tile (single or quad-ganged), and b) the study of the performance of the full readout chain. Point a) is currently being addressed by the T1604 Collaboration, with the construction and test of two front-end boards with four SiPMs ganged in active or hybrid mode. The performance of the full readout chain can be studied once a front-end board is available from CMS. That will occur probably in the second half of the next year. We anticipate that no more than one year would be necessary to complete this activity.

With the recent development of the hybrid RPCs by Beykent University team [85], significant changes in the operating conditions of the RPCs can be achieved in addition to the possibility to enhance the sensitivity of the RPCs to lower energetic particles. Further R&D is required to fully assess the feasibility of implementation of the new technique for REDTOP. We expect that approximately one year would be necessary to complete this activity.

F. Trigger

The present trigger architecture has been designed by CMS experts and it is based on several tests performed at Fermilab.Given the importance of this component of the experiment, a conservative estimate for completing the entire R&D on REDTOP trigger systems is about three years.

Level-0 As discussed in Sec. V E 4, the trigger logic needs to be tuned to accommodate the specifications of the HGCROC3 chip which is at the core of the readout of the calorimeter. Therefore, we foresee several tests and the construction of a demonstrator to verify that this component fulfils the requirements.

Level-1 A demonstrator of the Level-1 tracking trigger for CMS Phase II has shown that ten identical, FPGA-based, processors, housed in a single ATCA crate and operated in a time-multiplexing mode, can process events coming at a rate of 40 MHz from a unit corresponding to 1/48 of the CMS tracker. Each unit contained on the order of 500 hits carried by about 400 fibers. All the tracks with a P_t above 3 GeV/c could be reconstructed with high efficiency and a latency of a few microseconds. The rates processed and the complexity of the problem are on the same level as expected for the REDTOP Level-1 trigger.

Level-3 The Level-3 trigger is implemented entirely in software. Therefore, its full designed could be completed even at a later stage of the technical design of the experiment. Several algorithms are being tested as part of the ongoing sensitivity studies.

[1] P. J. V. et al., Eur. Phys. J. **A 56**, 183 (2020).
[2] G. Krnjaic, *Dark matter production at high intensities* (2020), URL https://indico.fnal.gov/event/44819/contributions/193751/attachments/132857/163535/RF6-Kickoff-DM-Production.pdf.
[3] B. Nefkens (1996), https://www.phy.bnl.gov/ags-2000/eta/eta.html, URL https://www.phy.bnl.gov/ags-2000/eta/eta.html.
[4] J. P. Singh and A. B. Patel, Journal of Physics G: Nuclear and Particle Physics **39**, 015006 (2011), URL https://doi.org/10.1088/0954-3899/39/1/015006.
[5] *The REDTOP experiment: Rare η/η' Decays To Probe New Physics* (2022), hep-ex/2203.07651.
[6] B. Batell, M. Pospelov, and A. Ritz, Phys. Rev. D **80**, 095024 (2009), URL https://link.aps.org/doi/10.1103/PhysRevD.80.095024.
[7] P. Langacker, Reviews of Modern Physics **81**, 1199 (2009), ISSN 1539-0756, URL http://dx.doi.org/10.1103/RevModPhys.81.1199.
[8] B. Holdom, Physics Letters B **166**, 196 (1986), ISSN 0370-2693, URL https://www.sciencedirect.com/science/article/pii/0370269386913778.
[9] J. N. Ng and D. J. Peters, Phys. Rev. D **46**, 5034 (1992), URL https://link.aps.org/doi/10.1103/PhysRevD.46.5034.
[10] J. N. Ng and D. J. Peters, Phys. Rev. D **47**, 4939 (1993), URL https://link.aps.org/doi/10.1103/PhysRevD.47.4939.
[11] E. Shabalin, Physica Scripta **T99**, 104 (2002), URL https://doi.org/10.1238/physica.topical.099a00104.
[12] R. Escribano and E. Royo, Eur. Phys. J. C **80**, 1190 (2020), [Erratum: Eur.Phys.J.C 81, 140 (2021)], 2007.12467.
[13] D. O'Connell, M. J. Ramsey-Musolf, and M. B. Wise, Phys. Rev. D **75-3**, 037701 (2007).
[14] S. Tulin, Phys. Rev. D **89**, 114008 (2014), 1404.4370.
[15] B. Batell, A. Freitas, A. Ismail, and D. Mckeen, Phys. Rev. D **100**, 095020 (2019), 1812.05103.
[16] F. Kling and S. Trojanowski, Phys. Rev. D **104**, 035012 (2021), 2105.07077.
[17] A. Anastasi et al. (KLOE-2), JHEP **05**, 019 (2016), 1601.06985.
[18] W. Abdallah, R. Gandhi, and S. Roy, Phys. Rev. D **104**, 055028 (2021), 2010.06159.
[19] R. D. Peccei and H. R. Quinn, Phys. Rev. D **16**, 1791 (1977), URL https://link.aps.org/doi/10.1103/PhysRevD.16.1791.
[20] R. D. Peccei and H. R. Quinn, Phys. Rev. Lett. **38**, 1440 (1977).
[21] S. Weinberg, Phys. Rev. Lett. **40**, 223 (1978), URL https://link.aps.org/doi/10.1103/PhysRevLett.40.223.
[22] F. Wilczek, Phys. Rev. Lett. **40**, 279 (1978), URL https://link.aps.org/doi/10.1103/PhysRevLett.40.279.
[23] W. A. Bardeen, R. D. Peccei, and T. Yanagida, Nucl. Phys. **B279**, 401 (1987).
[24] D. S. M. Alves and N. Weiner, JHEP **07**, 092 (2018), 1710.03764.
[25] D. S. Alves, Phys. Rev. **D 103, 055018** (2021).
[26] C. P. et al., Chinese Physics C **40**, 100001 (2016), URL https://doi.org/10.1088/1674-1137/40/10/100001.
[27] *Proceedings of the International Conference on Mesons and Nuclei at Intermediate Energie* (1994).
[28] S. Gardner and J. Shi, Phys. Rev. D **101**, 115038 (2020), URL https://link.aps.org/doi/10.1103/PhysRevD.101.115038.
[29] H. Akdag, T. Isken, and B. Kubis, JHEP **02**, 137 (2022), 2111.02417.
[30] J. G. Layter, J. A. Appel, A. Kotlewski, W. Lee, S. Stein, and J. J. Thaler, Phys. Rev. Lett. **29**, 316 (1972), URL https://link.aps.org/doi/10.1103/PhysRevLett.29.316.

[31] F. Ambrosino, A. Antonelli, M. Antonelli, F. Archilli, P. Beltrame, G. Bencivenni, S. Bertolucci, C. Bini, C. Bloise, S. Bocchetta, et al., Physics Letters B **675**, 283 (2009).
[32] P. Adlarson, W. Augustyniak, W. Bardan, M. Bashkanov, F. S. Bergmann, M. Berłowski, H. Bhatt, A. Bondar, M. Büscher, H. Calén, et al. (WASA-at-COSY Collaboration), Phys. Rev. C **90**, 045207 (2014), URL https://link.aps.org/doi/10.1103/PhysRevC.90.045207.
[33] P. Herczeg and P. Singer, Phys. Rev. D **8**, 4107 (1973), URL https://link.aps.org/doi/10.1103/PhysRevD.8.4107.
[34] C. Q. Geng, J. N. Ng, and T. H. Wu, Modern Physics Letters A **17**, 1489 (2002), ISSN 1793-6632, URL http://dx.doi.org/10.1142/S0217732302007697.
[35] D.-N. Gao, Modern Physics Letters A **17**, 1583 (2002).
[36] L. Gan, B. Kubis, E. Passemar, and S. Tulin, Phys. Rept. **945**, 2191 (2022), 2007.00664.
[37] P. Adlarson, W. Augustyniak, W. Bardan, M. Bashkanov, F. S. Bergmann, M. Berłowski, H. Bhatt, A. Bondar, M. Büscher, H. Calén, et al. (WASA-at-COSY Collaboration), Phys. Rev. C **94**, 065206 (2016), URL https://link.aps.org/doi/10.1103/PhysRevC.94.065206.
[38] P. Sanchez-Puertas, JHEP **01**, 031 (2019), 1810.13228.
[39] P. Zyla et al. (Particle Data Group), PTEP **2020**, 083C01 (2020).
[40] K. Kampf, J. Novotný, and P. Sanchez-Puertas, Phys. Rev. D **97**, 056010 (2018), 1801.06067.
[41] C. Jarlskog and H. Pilkuhn, Nucl. Phys. B **1**, 264 (1967).
[42] D. Guadagnoli, D. Melikhov, and M. Reboud, Phys. Lett. B **760**, 442 (2016), 1605.05718.
[43] A. A. Alves Junior et al., JHEP **05**, 048 (2019), 1808.03477.
[44] M. Borsato, V. V. Gligorov, D. Guadagnoli, D. Martinez Santos, and O. Sumensari, Phys. Rev. D **99**, 055017 (2019), 1808.02006.
[45] G. Lanfranchi, M. Pospelov, and P. Schuster, Ann. Rev. Nucl. Part. Sci. **71**, 279 (2021), 2011.02157.
[46] A. Datta, J. Liao, and D. Marfatia, Phys. Lett. B **768**, 265 (2017), 1702.01099.
[47] F. Sala and D. M. Straub, Phys. Lett. B **774**, 205 (2017), 1704.06188.
[48] A. Datta, J. Kumar, J. Liao, and D. Marfatia, Phys. Rev. D **97**, 115038 (2018), 1705.08423.
[49] A. K. Alok, B. Bhattacharya, A. Datta, D. Kumar, J. Kumar, and D. London, Phys. Rev. D **96**, 095009 (2017), 1704.07397.
[50] W. Altmannshofer, M. J. Baker, S. Gori, R. Harnik, M. Pospelov, E. Stamou, and A. Thamm, JHEP **03**, 188 (2018), 1711.07494.
[51] A. Datta, B. Dutta, S. Liao, D. Marfatia, and L. E. Strigari, JHEP **01**, 091 (2019), 1808.02611.
[52] L. Darmé, M. Fedele, K. Kowalska, and E. M. Sessolo, JHEP **08**, 148 (2020), 2002.11150.
[53] L. Darmé, M. Fedele, K. Kowalska, and E. M. Sessolo (2021), 2106.12582.
[54] P. Masjuan and P. Sanchez-Puertas, JHEP **08**, 108 (2016), 1512.09292.
[55] H. E. Haber, in *21st Annual SLAC Summer Institute on Particle Physics: Spin Structure in High-energy Processes (School: 26 Jul - 3 Aug, Topical Conference: 4-6 Aug) (SSI 93)* (1994), pp. 231–272, hep-ph/9405376.
[56] R. Escribano, E. Royo, and P. Sanchez-Puertas (2022), 2202.04886.
[57] A. D. Sakharov, Soviet Journal of Experimental and Theoretical Physics Letters **5**, 24 (1967).
[58] A. P. Zhitnitskii, Sov. J. Nucl. Phys. (Engl. Transl.); (United States) **31** (1980), URL https://www.osti.gov/biblio/7063072.
[59] I. I. Bigi and A. I. Sanda, *CP Violation*, vol. Nuclear Physics and Cosmology, Series (Cambridge Monographs on Particle Physics, 1999).
[60] V. Efrosinin, I. Khriplovich, G. Kirilin, and Y. Kudenko, Physics Letters B **493**, 293 (2000), ISSN 0370-2693, URL http://dx.doi.org/10.1016/S0370-2693(00)01167-9.
[61] R. Garisto and G. Kane, Physical Review D **44**, 2038 (1991).
[62] G.-H. Wu and J. N. Ng, Physics Letters B **392**, 93 (1997), ISSN 0370-2693, URL http://dx.doi.org/10.1016/S0370-2693(96)01538-9.
[63] M. Albaladejo et al. (JPAC) (2021), 2112.13436.
[64] D. S. M. A. et al., Eur. Phys. J. C **83**, 230 (2023).

[65] C. Collaboration, *Observation of the rare decay of the η meson to four muons* (2023), 2305.04904.

[66] H.-B. Li, Journal of Physics G: Nuclear and Particle Physics **36**, 085009 (2009), URL https://doi.org/10.1088%2F0954-3899%2F36%2F8%2F085009.

[67] C. Gatto, *The geniehad event generation framework.* (2012), URL https://redtop.fnal.gov/the-geniehadevent-generation-framework.

[68] K. Arndt, H. Augustin, P. Baesso, N. Berger, F. Berg, C. Betancourt, D. Bortoletto, A. Bravar, K. Briggl, D. vom Bruch, et al., Nuclear Instruments and Methods in Physics Research Section A: Accelerators, Spectrometers, Detectors and Associated Equipment **1014**, 165679 (2021), ISSN 0168-9002.

[69] A. Blondel et al., *Research proposal for an experiment to search for the decay $\mu \to eee$* (2012), URL https://www.psi.ch/sites/default/files/import/mu3e/DocumentsEN/ResearchProposal.pdf.

[70] T. Rudzki, H. Augustin, M. Deflorin, S. Dittmeier, F. Frauen, D. M. Immig, D. Kim, F. M. Aeschbacher, A. M. GonzÃ¡lez, M. Menzel, et al., *The mu3e experiment: Toward the construction of an hv-maps vertex detector* (2021), 2106.03534.

[71] ATLAS Collaboration (2020), URL https://cds.cern.ch/record/2719855.

[72] CMS Collaboration (2019), URL http://cds.cern.ch/record/2667167.

[73] C. Gatto, J. Phys.: Conf. Ser. **587**, 012060 (2015).

[74] C. Gatto, J. Phys.: Conf. Ser. **404**, 012030 (2015).

[75] e. a. I. Belyaev, The European Physical Journal **H 46** (2021).

[76] G. Deputch et al. (2011).

[77] P. Paschos, *Redtop computing model* (2022), URL http://redtop.fnal.gov/wp-content/uploads/2020/05/redtop-compute_v3.pdf.

[78] M. Bertani et al., Nuclear Physics B (Proc. Suppl.) **78**, 553 (1999).

[79] GoodFellow, *99.8% beryllium foil 0.025mm thick* (2023), URL https://www.goodfellow.com/p/be00-fl-000120/beryllium-foil.

[80] A. Schoening, *Private communication* (2023).

[81] Tech. Rep., CERN, Geneva (2017), URL https://cds.cern.ch/record/2293646.

[82] D. Barney, *The high granularity calorimeter for cms* (2018), URL https://agenda.infn.it/event/14816/contributions/26692/.

[83] C. Adams, A. Bambaugh, B. Bilki, J. Butler, F. Corriveau, T. Cundiff, G. Drake, K. Francis, B. Furst, V. Guarino, et al., Journal of Instrumentation **11**, P07007 (2016), URL https://dx.doi.org/10.1088/1748-0221/11/07/P07007.

[84] URL https://twiki.cern.ch/twiki/bin/view/CALICE/WebHome.

[85] M. Tosun, B. Bilki, and K. Sahbaz, Nuclear Instruments and Methods in Physics Research Section A: Accelerators, Spectrometers, Detectors and Associated Equipment **1054**, 168448 (2023), ISSN 0168-9002, URL https://www.sciencedirect.com/science/article/pii/S0168900223004382.